SP 0825

Time Domain Simulation of Airfoil Flutter in the Subsonic Regime using Fluid Structure Coupling Through Panel Method

SOMENATH MUKHERJEE, M MANJUPRASAD,
NEERAJ KUMAR SHARMA, DAVINDER RANA,
AMIT KUMAR ONKAR
Structural Technologies Division

Special Publication STTD 0825
December 2008

National Aerospace Laboratories
Bangalore 560 017, India

CONTENTS

1. INTRODUCTION

Aeroelasticity is the science which studies the interaction among aerodynamics, inertia and elastic forces. Modern airplane structures are not completely rigid, and aeroelastic phenomena arise when structural deformations induce changes on aerodynamic forces. The additional aerodynamic forces from some sort of perturbation cause increase in the structural deformations, which lead to greater aerodynamic forces. These interactions may become smaller until a condition of equilibrium is reached, or may diverge catastrophically. Aeroelasticity can generally be divided in two fields of study:

Static aeroelasticity
Dynamic aeroelasticity

Static aeroelasticity
Static aeroelasticity studies the interaction between aerodynamics and elastic forces on an elastic structure. Mass properties are not significant in the calculations of this type of phenomena.

Dynamic aeroelasticity
Dynamic aeroelasticity studies the interactions among unsteady aerodynamic, elastic, and inertial forces. An example of dynamic aeroelastic phenomena is *flutter*, in which the flexibility and inertia of the structure plays an essential part in the dynamic stability of the total fluid-structure system. It occurs when a structural system is driven into self-exciting oscillations due to *unsteady* aerodynamic forces from the flow, and is characterised by *unstable* oscillations of a flexible structure. Beyond certain critical flow conditions, the onset of flutter instability is recognised by the increase in the vibration amplitudes of the structural system with time (Figure 1). Aircraft structures that function as lifting surfaces are prone to flutter instability due to their interaction with the aerodynamic loads.

The critical flow condition that leads to the onset of flutter is called as the 'Flutter Boundary' of the structure subjected to the type of aerodynamic flow. The flutter boundary of an aerospace vehicle is a characteristic design parameter that is very important for practical design of its lifting surfaces.

1.1 Objectives of the present work

The primary objective of the present work is the development of a working algorithm and a computer code in FORTRAN for dynamic *coupling* of the airfoil structure to a two-dimensional *subsonic* aerodynamic flow, so that the aeroelastic motion of the airfoil in the flow can be simulated in the time domain. The intention is to determine the flutter boundary of the airfoil through a time domain analysis, using a simple two-dimensional aerodynamic code based on panel methods, suitably *coupled* to the airfoil structural code.

For the purpose, a panel code for the subsonic incompressible flow is prepared, and a compressibility correction factor for the aerodynamic forces is incorporated. The symmetric *NACA 0012* airfoil is chosen to first simulate the steady subsonic flow conditions. The pressure distributions, their integrated values of moment coefficients and the centre of pressure for this airfoil section are determined for various angles of attack. The steady flow results generated for subsonic flow agree well with analytical solutions of subsonic incompressible and non-viscous flows.

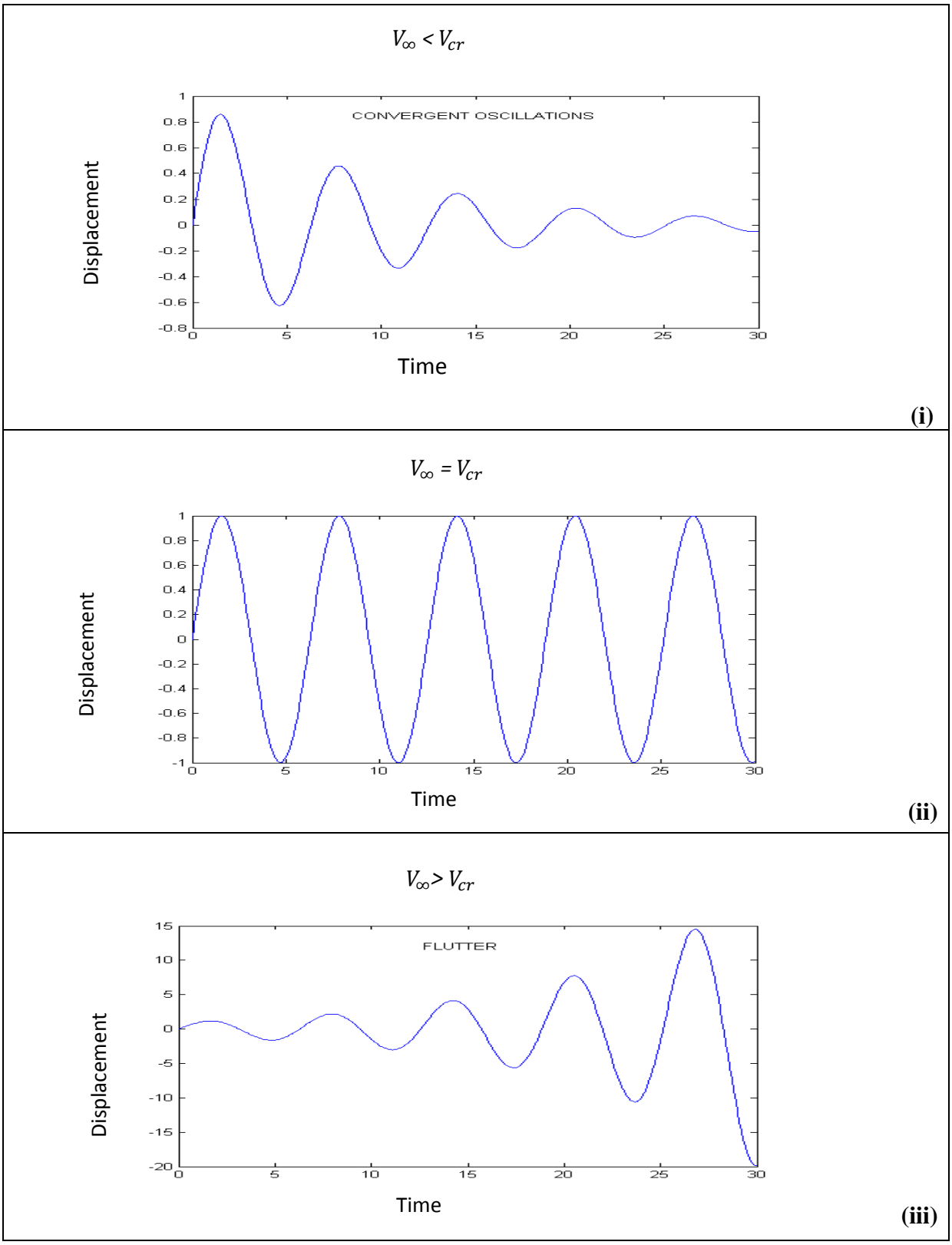

Figure 1. Nature of dynamic response (displacement) of a structural system subjected to aerodynamic flow. For free stream flow velocities below a critical value, $V_\infty < V_{cr}$, the oscillations are stable, as shown in (i). At the critical flow velocity, the oscillations are un-damped, as shown in (ii). For velocities above this critical value, $V_\infty > V_{cr}$, the oscillations are unstable, as shown in (iii).

The airfoil stiffness characteristics adopted here are intentionally chosen so that it has a subsonic flutter boundary. The inertia properties of the airfoil are typical values, and do not necessarily conforms to the actual values of the *NACA 0012* airfoil. The results are generated for a *unit* width and *unit* chord length of the airfoil.

1.2 Summary of the present work.

The present work starts with brief presentation of the fundamental concepts and derivation of the relevant equations of motion of the airfoil in airflow. The airfoil is considered as a rigid section, supported by translational and rotational springs at a point in its chord(c), so that only heave and pitch degrees of freedom are permitted at the point of support.

First, the classical method, based on the direct eigenvalue approach [1, 2], is used to solve the equations of motion of an un-damped system and to determine the flutter boundary of the airfoil. The lift gradient with respect to angle of attack is maintained as prescribed by the classical, incompressible, non-viscous aerodynamic theory [1-4]. This work is followed by another in which damping from viscous effects and aerodynamic flow are incorporated and the solution is obtained by using the state space technique. The Theodorsen's function *C(k)* is also incorporated to simulate the phase difference between the aerodynamic forces and the airfoil response, and the *p-k* method is adopted for solution.

To solve the equation of motion in the time domain using Newmark's implicit method, a mathematical algorithm of the coupling of airfoil with the airflow is developed. The coupling algorithm between the airfoil dynamics and the aerodynamic flow is directly adopted from the reports prepared at DLR in Gottingen, Germany, that deals with *transonic limit cycle oscillations* of airfoils beyond the flutter boundary [5, 6]. Furthermore, a panel code, in the form of a subroutine, is developed here to simulate the aerodynamic flow and the forces. Newmark's method has also been applied for simulating time history of response of aircraft wings to gust loads of some assumed time history [2, 7].

Results of the present analysis in the time domain are simulated to show the behaviour of the airfoil in the subsonic flow. Stable and unstable oscillations are shown graphically. Critical conditions, signifying the flutter boundary, are identified for the flow velocity at which the motion of the unstable mode is just simple harmonic, without any decay or increase of amplitude in time. Beyond the critical condition, the oscillation amplitudes grow with time.

The panel code is used to simulate the time history of flow parameters for a typical symmetric airfoil (NACA 0012). It computes the pressure coefficients C_p over the top and bottom surfaces of the airfoil, lift L, lift coefficient C_L, position of centre of pressure and the pitching moment M about the support point. These data are passed onto the structural code that evaluates the dynamic support displacements (heave h and pitch α), about the *mean position* in the time domain. These displacements are then taken into the panel code to recalculate the aerodynamic forces. This process is continued and the response of the airfoil in the time domain is determined.

Finally, a pseudo-aerodynamic code is also prepared and coupled with the structural code of the airfoil. In this code, an *assumed* value of the lift gradient ($dC_L/d\alpha$) is used and the centre of pressure is assumed to be at the quarter chord point from the leading edge of the airfoil [1, 4]. No pressure distributions over the airfoil are actually generated by this code.

Flutter frequencies and flutter velocities obtained by the various methods are then compared. There is a good agreement of the results by the various methods. The present

analysis with a simple airfoil coupled to a 2D subsonic flow (simulated by the panel method) indicates that it is possible, in principle, to simulate flutter even in the transonic and supersonic regimes, using more sophisticated aerodynamic codes (*i.e.* solving Navier Stokes equations).

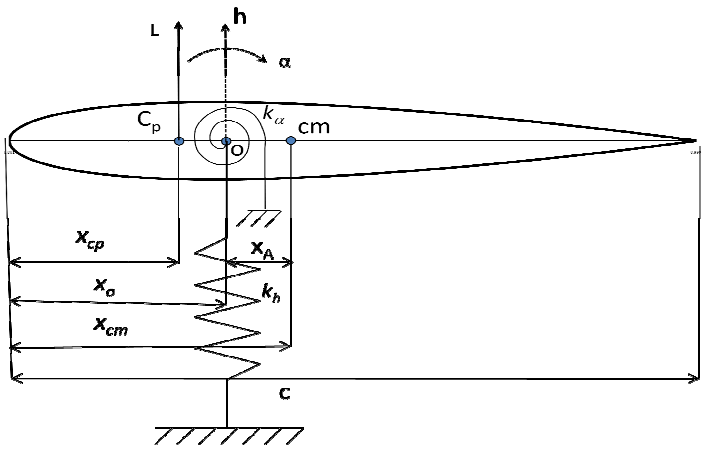

Figure 2. A typical section of an airfoil

2. EQUATION OF MOTION OF THE AIRFOIL

A typical cross section of an airfoil (for a hypothetical wing of infinite span) is shown in Figure 2. This justifies a two-dimensional aerodynamic flow around it. The airfoil properties correspond to *per unit span* (for this infinite wing) which basically remain same at any arbitrary location of the section along the span. Here c is the chord length of the airfoil X_{cp} is the position of *centre of pressure*, X_{cm} is the position of *centre of mass* and X_0 is the position of the *centre of flexural axis*, h and α denote the *heave* and *pitch* displacements (positive nose up) respectively of point O. The integrated aerodynamic forces are *lift, L* (positive upwards) and *pitching moment M* (positive nose up) act at the flexural point O. The mass moment of inertia of the section about the flexure axis (point of support O) is given by I_α. The spring stiffness in heave and pitch motions are respectively denoted by K_h and K_α, while the corresponding structural damping coefficients are denoted by C_h and C_α.

For the airfoil section of mass m and moment of inertia about the center of mass I_{cm} per unit span, the kinetic energy T is given by:

$$T = \frac{1}{2}m\left(\dot{h} - X_A\dot{\alpha}\right)^2 + \frac{1}{2}I_{cm}\dot{\alpha}^2 \qquad \text{where } X_A = (X_{cm} - X_O)$$

The potential energy V of the system is given by:

$$V = \frac{1}{2}K_h h^2 + \frac{1}{2}K_\alpha \alpha^2$$

Hence, the Lagrangian is given by

$$\mathcal{L} = T - V = \frac{1}{2}m\left(\dot{h} - X_A\dot{\alpha}\right)^2 + \frac{1}{2}I_{cm}\dot{\alpha}^2 - \frac{1}{2}K_h h^2 - \frac{1}{2}K_\alpha \alpha^2$$

The equation of motion for the airfoil with two degrees of freedom (heave 'h', and pitch 'α') can now be obtained using the Lagrange's equation (for conservative system) as:

$$\frac{d}{dt}\frac{\partial \mathcal{L}}{\partial \dot{h}} - \frac{\partial \mathcal{L}}{\partial h} = L$$

$$\frac{d}{dt}\frac{\partial \mathcal{L}}{\partial \dot{\alpha}} - \frac{\partial \mathcal{L}}{\partial \alpha} = M$$

This leads to the following equation of motion for the airfoil

$$\begin{bmatrix} m & -mX_A \\ -mX_A & I_\alpha \end{bmatrix} \begin{Bmatrix} \ddot{h} \\ \ddot{\alpha} \end{Bmatrix} + \begin{bmatrix} K_h & 0 \\ 0 & K_\alpha \end{bmatrix} \begin{Bmatrix} h \\ \alpha \end{Bmatrix} = \begin{Bmatrix} L \\ M \end{Bmatrix} \tag{2.1}$$

or

$$[\mathcal{M}]\{\ddot{u}\} + [K]\{u\} = \{F\} \tag{2.2}$$

where $\{u\}=\{h, \alpha\}^{\mathrm{T}}$ and $\{F\}$ denote the displacement and force vectors respectively whereas $[\mathcal{M}]$ and $[K]$ denote the mass and stiffness matrices respectively. These matrices are given by

$$[\mathcal{M}] = \begin{bmatrix} m & -mX_A \\ -mX_A & I_\alpha \end{bmatrix} \qquad [K] = \begin{bmatrix} K_h & 0 \\ 0 & K_\alpha \end{bmatrix} \qquad \text{and} \qquad \{F\} = \begin{Bmatrix} L \\ M \end{Bmatrix} \tag{2.3}$$

Here $I_\alpha = I_{cm} + m\,{X_A}^2$ is the mass moment of inertia of the airfoil section (of unit width) about the point of support O. Note that the stiffness matrix is diagonal because the point of support is at the flexural centre, where the heave and the pitch are statically uncoupled. Since the centre of mass is away from the point of support there is an inertial coupling in the mass matrix.

The aerodynamic lift and pitching moment about the point of support *O* per unit span are given by the expressions as:

$$L = \frac{1}{2}\rho_\infty V_\infty^2 c C_L = \frac{1}{2}\rho_\infty V_\infty^2 c \, \frac{\partial C_L}{\partial \alpha}\alpha_{eff} \tag{2.4}$$

where α_{eff} is the effective unsteady angle of attack.

and $M = \frac{1}{2}\rho_\infty V_\infty^2 c C_L (X_O - X_{cp}) = \frac{1}{2}\rho_\infty V_\infty^2 c C_L\,(lc)$ where $lc = X_O - X_{cp}$

$$= \frac{1}{2}\rho_\infty V_\infty^2 c^2 \frac{\partial C_l}{\partial \alpha}\alpha_{eff} l = C_m \frac{1}{2}\rho_\infty V_\infty^2 c^2 \tag{2.5}$$

where $C_L = \frac{\partial C_L}{\partial \alpha}\alpha_{eff}$, $C_m = \frac{\partial C_l}{\partial \alpha}\alpha_{eff}\, l$, are the lift and moment coefficients (about the support point O) respectively, c is the chord length of the section, ρ_∞ is the free stream air density and V_∞ is the free stream flow velocity. Compressibility correction factors, suggested by Prandtl and Glauert, are incorporated to determine the aerodynamic coefficients from those values determined through the incompressible flow theory.

$$C_p(\text{compressible}) = \frac{C_p(\text{incompressible})}{\sqrt{1 - M_\infty^2}}$$

$$C_L(\text{compressible}) = \frac{C_L(\text{incompressible})}{\sqrt{1 - M_\infty^2}}$$

$$C_m(\text{compressible}) = \frac{C_m(\text{incompressible})}{\sqrt{1-M_\infty^2}} \tag{2.6}$$

where $M_\infty = \frac{V_\infty}{a_{sound}}$ is the free stream Mach number. Here a_{sound} represents the isentropic velocity of sound in a gas, given by the expression $a_{sound} = \sqrt{\gamma RT}$, where γ is the isentropic index (specific heat ratio) of the gas, R is the corresponding gas constant, and T is the gas temperature. For air, γ=1.4, and R=287 J kg^{-1} K^{-1}. Thus for the free stream flow of air, of assumed ambient temperature T=T_∞=288.16 K, the velocity of sound is $a_{sound} =$ 340.26 m/sec. The lift gradient for the infinite thin airfoil in a two-dimensional incompressible flow is $\partial C_L/\partial\alpha = 2\pi$. A corrected set of expressions for the lift and moment coefficients (about support point) with compressibility effects considered is given by

$$C_L = \frac{\partial C_L}{\partial \alpha}\alpha_{eff}, \qquad \frac{\partial C_L}{\partial \alpha} = \frac{2\pi}{\sqrt{1-M_\infty^2}} \tag{2.7a}$$

Pitching moment coefficient about any point (at distance X from the leading edge) is

$$C_{m_X} = \frac{M_X}{\frac{1}{2}\rho_\infty V_\infty^2 c^2} \tag{2.7b}$$

Pitching moment coefficient about the support (X=X_O)

$$C_m = \frac{M}{\frac{1}{2}\rho_\infty V_\infty^2 c^2} \tag{2.7c}$$

For non conservative system, Lagrangian equation becomes

$$\frac{d}{dt}\frac{\partial \mathcal{L}}{\partial \dot{u}_i} - \frac{\partial \mathcal{L}}{\partial u_i} + \frac{\partial (DE)}{\partial \dot{u}_i} = F_i$$

where DE is the dissipation energy of the system. By defining $DE = \frac{1}{2}C_h\dot{h}^2 + \frac{1}{2}C_\alpha\dot{\alpha}^2$ we get the above equation in matrix form as

$$\begin{bmatrix} m & -mX_A \\ -mX_A & I_\alpha \end{bmatrix}\begin{Bmatrix}\ddot{h}\\ \ddot{\alpha}\end{Bmatrix} + \begin{bmatrix} C_h & 0 \\ 0 & C_\alpha \end{bmatrix}\begin{Bmatrix}\dot{h}\\ \dot{\alpha}\end{Bmatrix} + \begin{bmatrix} K_h & 0 \\ 0 & K_\alpha \end{bmatrix}\begin{Bmatrix}h\\ \alpha\end{Bmatrix} = \begin{Bmatrix}L\\ M\end{Bmatrix} \tag{2.8}$$

or $$[\mathcal{M}]\{\ddot{u}\} + [D]\{\dot{u}\} + [K]\{u\} = \{F\} \tag{2.9}$$

where $[D] = \begin{bmatrix} C_h & 0 \\ 0 & C_\alpha \end{bmatrix}$ is the damping matrix.

In principle, the aerodynamic forces in the equation of motion (2.8) should be unsteady in nature. Thus suitable unsteady aerodynamic codes should be used to generate these forces in time. In this report, appropriate modifications in the steady expressions for these forces in the classical strip theory formulation have been made to incorporate the unsteady nature of the flow. This modification, incorporated only for the classical flutter analysis, effectively considers the *aerodynamic damping* terms involving the heave and pitch velocity components, which influence the effective angle of attack. Thus the airfoil is subjected to aerodynamic damping, in addition to its own structural/viscous damping.

Furthermore, a correction factor for unsteady effects using Theodorsen's function [1] has also been incorporated in the classical methods. However, for the time domain solutions of the equation of motion of the airfoil using the in-house developed panel code, no unsteady effects at all have been considered. Unsteady effects for such time domain problems will be simulated in the future with a suitable unsteady code.

3. METHODS OF ANALYSIS

The equations of motion presented in the previous section (equations (2.1) and (2.8)) have been solved here by the following methods.

a) Classical method (Direct eigenvalue method for the second order differential equation for the undamped case and the state space method for the equivalent first order equation for the damped case).

b) Time simulation (Direct integration approach).

3.1 Classical methods

3.1.1. Direct eigenvalue approach for the undamped case

In this method the damping effects are not taken into account and the airfoil motion is governed by equation (2.1). This simplified approach can give a first estimate of the flutter boundary. Steady aerodynamic expressions are used here to approximate the unsteady aerodynamic loads without incorporating the aerodynamic damping terms. The corrected lift gradient for compressibility effects is given by equation (2.7). The elastic dynamic pitch is used as the effective angle of attack, ($\alpha_{eff} = \alpha$).

Hence the equation of motion (2.1) with the aerodynamic forces of equations (2.4) and (2.5) reduces to the form

$$\begin{bmatrix} m & -mX_A \\ -mX_A & I_\alpha \end{bmatrix} \begin{Bmatrix} \ddot{h} \\ \ddot{\alpha} \end{Bmatrix} + \begin{bmatrix} K_h & 0 \\ 0 & K_\alpha \end{bmatrix} \begin{Bmatrix} h \\ \alpha \end{Bmatrix} = \frac{1}{2}\rho_\infty V_\infty^2 c \ \frac{\partial C_L}{\partial \alpha} \begin{Bmatrix} \alpha \\ lc\ \alpha \end{Bmatrix} \tag{3.1}$$

where the lift gradient $\frac{\partial C_L}{\partial \alpha}$ of an airfoil in compressible flow is given by equation (2.7a). The time dependent displacement vector is expressed in the following form as:

$$\begin{Bmatrix} h \\ \alpha \end{Bmatrix} = \begin{Bmatrix} h_0 \\ \alpha_0 \end{Bmatrix} e^{\lambda t} \tag{3.2}$$

After substituting the above displacement vector into equation (3.1) we get,

$$\left[\begin{bmatrix} m & -mX_A \\ -mX_A & I_\alpha \end{bmatrix} \lambda^2 + \begin{bmatrix} K_h & 0 \\ 0 & K_\alpha \end{bmatrix} + \frac{1}{2}\rho_\infty V_\infty^2 c \ \frac{\partial C_l}{\partial \alpha} \begin{bmatrix} 0 & -1 \\ 0 & -(X_O - X_{cp}) \end{bmatrix} \right] \begin{Bmatrix} h_0 \\ \alpha_0 \end{Bmatrix} = \begin{Bmatrix} 0 \\ 0 \end{Bmatrix}$$

In matrix form, the above equation can be expressed as

$$\left[[K] + [A] + \lambda^2[\mathcal{M}]\right]\begin{Bmatrix} h_0 \\ \alpha_0 \end{Bmatrix} = 0 \tag{3.3}$$

where $[A]$ is the aerodynamic matrix, given by

$$[A] = \frac{1}{2}\rho_\infty V_\infty^2 c \ \frac{\partial C_l}{\partial \alpha}\begin{bmatrix} 0 & -1 \\ 0 & -(X_O - X_{cp}) \end{bmatrix} \tag{3.4}$$

3.1.1.1 Stability conditions

For non-trivial solution for the amplitudes, it implies from equation (3.3) that

$$Det\left[[K] + [A] + \lambda^2[\mathcal{M}]\right] = 0 \tag{3.5}$$

Three conditions may arise, depending on the value of free stream flow conditions.

Case 1. At subcritical flow velocities, in the absence of damping, both eigen values $(-\lambda^2)$ are real and positive, and therefore λ^2 values are real and negative, *i.e.* parameter $\lambda = \pm i\omega$ is purely imaginary. Two corresponding distinct values of purely imaginary λ yield the circular frequencies of the two modal branches in radians/sec. The system vibrates steadily with simple harmonic motion in each of the two branches arising from the natural (free vibration) modes. The frequencies in cycles/sec (or Hz) are given by $f = \frac{\omega}{2\pi}$

Case 2. Beyond a critical velocity, ($V_\infty > V_{cr}$) the parameters λ occur as complex conjugates, ($\lambda = \lambda_r \pm i\lambda_i$) with one of them having a positive real part ($\lambda_r > 0$). This implies that the oscillations of the appropriate modal branch are unstable, characterized by increase in amplitude with time. At the critical velocity ($V_\infty = V_{cr}$) *i.e.* at the flutter boundary, λ_r=0, indicating purely simple harmonic motion.

Case 3. Divergence instability is indicated by the condition that the imaginary part of λ vanishes, *i.e.* λ_i=ω=0.

3.1.2 State space method for the damped case

In this method, damping from viscous effects and unsteady aerodynamic flows are taken into account. The aerodynamic damping is incorporated through heave and pitch velocities in accordance with the following updated expressions for the unsteady aerodynamic forces about the point of support O, as suggested by Fung [1],

$$L = \frac{1}{2}\rho_\infty V_\infty^2 c C_L = \frac{1}{2}\rho_\infty V_\infty^2 c \ \frac{\partial C_L}{\partial \alpha}\alpha_{eff} \tag{3.6}$$

and $$M = L\left(X_O - X_{cp}\right) - \frac{1}{2}\rho_\infty V_\infty^2 c \ \frac{\partial C_L}{\partial \alpha}\left(\frac{c^2}{16V_\infty}\right)\dot{\alpha} \tag{3.7}$$

Here the *effective angle of attack* for the computation of these unsteady aerodynamic forces is given by the following expression

$$\alpha_{eff} = \alpha - \frac{1}{V_\infty}\dot{h} + \frac{1}{V_\infty}\left(\frac{3}{4}c - X_0\right)\dot{\alpha} \tag{3.8}$$

This is in accordance with the assumption that the lifting (vortex) line is located at the quarter chord, and the downwash condition is satisfied at the three-quarter chord. With these modifications, the equation of motion for the damped system can be expressed in the following form

$$\left[[K]+[A]\right]\begin{Bmatrix}h\\ \alpha\end{Bmatrix}+[\mathcal{M}]\begin{Bmatrix}\ddot{h}\\ \ddot{\alpha}\end{Bmatrix}+\left[[D]+[D_A]\right]\begin{Bmatrix}\dot{h}\\ \dot{\alpha}\end{Bmatrix}=\begin{Bmatrix}0\\ 0\end{Bmatrix} \tag{3.9}$$

where

$$[A]=\tfrac{1}{2}\rho_\infty V_\infty^2 c\ \ \frac{\partial C_l}{\partial \alpha}\begin{bmatrix}0 & -1\\ 0 & -(X_O-X_{cp})\end{bmatrix}$$

$$[D_A]=\frac{1}{2}\rho_\infty V_\infty^2 c\ \ \frac{\partial C_L}{\partial \alpha}\begin{bmatrix}\dfrac{1}{V_\infty} & -\dfrac{\left(\frac{3}{4}c-X_0\right)}{V_\infty}\\ \dfrac{(X_O-X_{cp})}{V_\infty} & -\dfrac{(X_O-X_{cp})\left(\frac{3}{4}c-X_0\right)}{V_\infty}+\dfrac{c^2}{16V_\infty}\end{bmatrix}$$

(3.10)

Here $[D_A]$ is the aerodynamic damping matrix. Equation (3.9) can now be expressed in the state space form as

$$\{\dot{x}\}=[S]\{x\}$$

where $[S]=\begin{bmatrix}0 & 0 & 1 & 0\\ 0 & 0 & 0 & 1\\ -[\mathcal{M}]^{-1}[K+A] & & -[\mathcal{M}]^{-1}\left[[D]+[D_A]\right] & \end{bmatrix}$ and $\{x\}=\begin{Bmatrix}h\\ \alpha\\ \dot{h}\\ \dot{\alpha}\end{Bmatrix}$ (3.11)

Using $\{\dot{x}\}=\lambda\{x\}$, we have the following form from the above equation

$$[S]\{x\}=\lambda\{x\}$$

or $$\left[[S]-\lambda[I]\right]\{x\}=\{0\} \tag{3.12}$$

where $[I]$ is the identity matrix.

For non trivial solutions, we have the following eigenvalue problem,

$$Det\left[[S]-\lambda[I]\right]=0 \tag{3.13}$$

Theodorsen's function and the p-k method of analysis

The Jones formula [1] for the frequency dependent Theodorsen's complex function *C(k)* is used here to introduce the phase difference between the aerodynamic loading and the

response. This is achieved by updating the aerodynamic matrices $[A]$ and $[D_A]$ by multiplying these by the function $C(k)$,

$$C(k) = 1 - \frac{0.165}{1 - \frac{0.0455}{k}i} - \frac{0.335}{1 - \frac{0.3}{k}i} \tag{3.14}$$

where $k = \frac{c\omega}{2V_\infty}$ is the non-dimensional reduced frequency obtained from the imaginary part of the eigenvalue λ. Convergence in k values for each modal branch is achieved through an iterative method for a given flow velocity. The flow chart for the above *p-k* algorithm is presented in Figure 3. Here the updated aerodynamic matrix $[A]$ and the updated aerodynamic damping matrix $[D_A]$ are given as

$$[A] = C(k)\times\frac{1}{2}\rho_\infty V_\infty^2 c \ \frac{\partial C_l}{\partial \alpha}\begin{bmatrix} 0 & -1 \\ 0 & -(X_O - X_{cp}) \end{bmatrix} \tag{3.15}$$

$$[D_A] = C(k)\times\frac{1}{2}\rho_\infty V_\infty^2 c \ \frac{\partial C_L}{\partial \alpha}\begin{bmatrix} \frac{1}{V_\infty} & -\frac{\left(\frac{3}{4}c - X_0\right)}{V_\infty} \\ \frac{(X_O - X_{cp})}{V_\infty} & -\frac{(X_O - X_{cp})\left(\frac{3}{4}c - X_0\right)}{V_\infty} + \frac{c^2}{16V_\infty} \end{bmatrix} \tag{3.16}$$

3.1.2.1 Stability conditions

Case 1. At subcritical flow velocities in the presence of damping, all the eigenvalues are complex, $\lambda = \lambda_r \pm i\lambda_i = (-\zeta\omega \pm i\omega)$, with *negative real* parts, $\lambda_r < 0$, indicating that the net effective damping ζ is *positive*, (since $\omega > 0$), leading to stable oscillations, characterized by *decrease* in amplitude with time. The imaginary parts of the eigenvalues give the circular frequencies ($\lambda_i = \omega$ in radians/sec) of the associated branches from the two modes, while the real parts give the time dependence of the amplitudes.

Case 2. Beyond a critical velocity, ($V_\infty > V_{cr}$), the *real* part of at least one of the complex eigenvalues, $\lambda = (-\zeta\omega \pm i\omega)$, becomes *positive*, *i.e.* $\lambda_r = -\zeta\omega > 0$. This indicates that beyond this critical velocity, the *net* damping ζ is *negative,* leading to unstable oscillations, characterized by i*ncrease* in amplitude with time. At the *critical* (flutter) velocity ($V_\infty = V_{cr}$) *i.e.* at the flutter boundary, the real part of the eigenvalues vanishes, ($\lambda_r = 0$), indicating purely simple harmonic motion, without any net damping at all.

Case 3. Divergence is indicated by the condition that the imaginary part of λ vanishes, *i.e.* $\lambda_i = \omega = 0$.

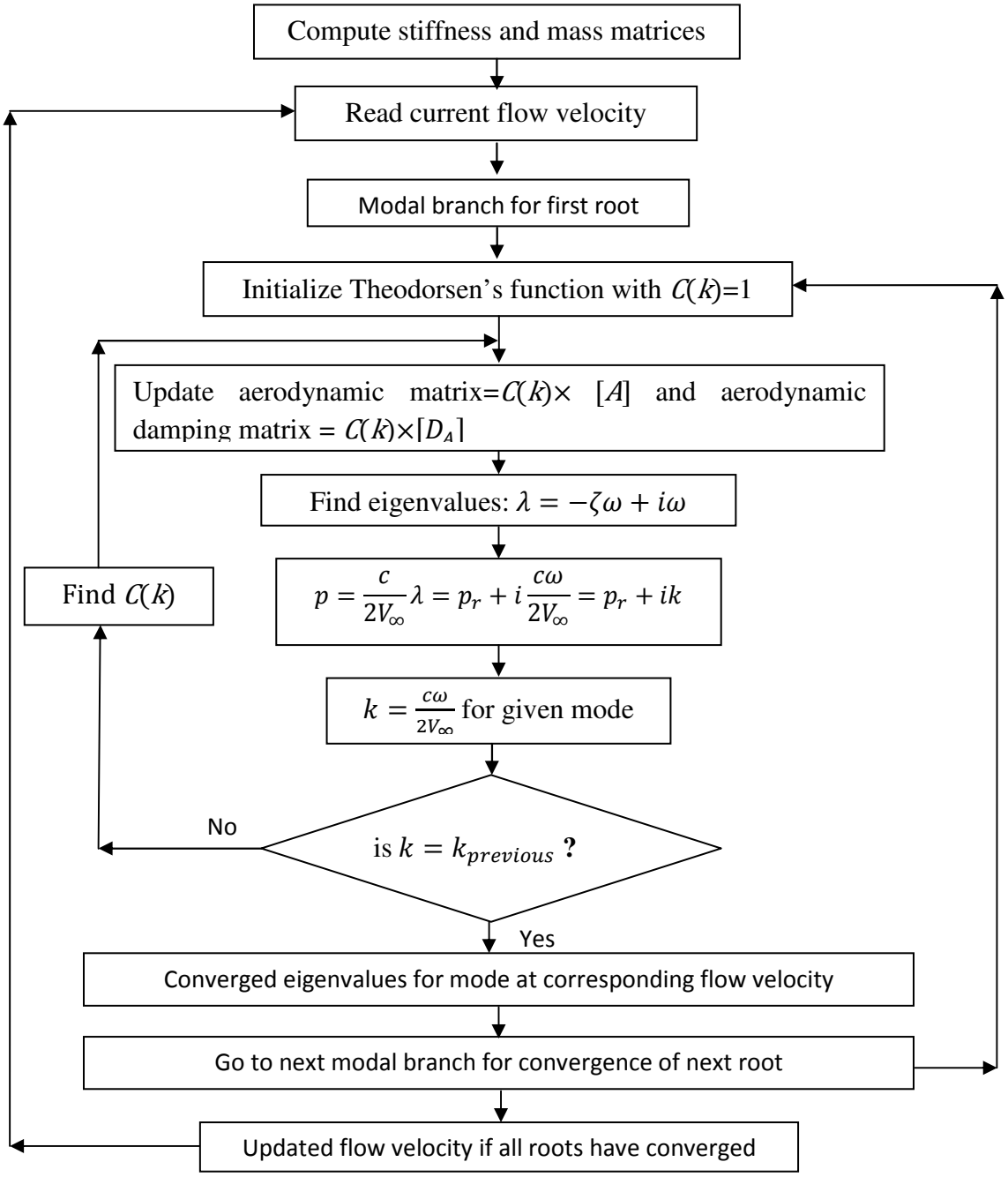

Figure 3. Algorithm for *p-k* Method.

3.2 Time history simulation approach

In this approach structural damping is taken into account, so the equation of motion is governed by equation (2.8) as:

$$\begin{bmatrix} m & -mX_A \\ -mX_A & I_\alpha \end{bmatrix}\begin{Bmatrix} \ddot{h} \\ \ddot{\alpha} \end{Bmatrix} + \begin{bmatrix} C_h & 0 \\ 0 & C_\alpha \end{bmatrix}\begin{Bmatrix} \dot{h} \\ \dot{\alpha} \end{Bmatrix} + \begin{bmatrix} K_h & 0 \\ 0 & K_\alpha \end{bmatrix}\begin{Bmatrix} h \\ \alpha \end{Bmatrix} = \begin{Bmatrix} L \\ M \end{Bmatrix} \tag{3.17}$$

In order to solve the above equation, the aerodynamic forces (L and M) are obtained by two different methods to simulate the dynamics of the airfoil.

(a) Panel method.

(b) Assumed lift gradient and centre of pressure at quarter chord point (c/4).

In this approach no aerodynamic damping is considered, and the steady formulations have been directly employed as quasi-steady ones to generate the unsteady aerodynamic forces (equations (2.4) and (2.5)) in the time domain through proper coupling algorithm to the structural response.

3.2.1 Panel method

The panel method for estimating the aerodynamic loads is actually based on the steady flow conditions, but the method is adopted also for estimating unsteady aerodynamic loads by assuming small unsteady (dynamic) perturbations about the steady (or mean) configuration of the airfoil. First we consider the steady configuration of the airfoil, subjected to a *steady relative* wind V_∞, for a steady angle of attack α, as shown in Figure 4. The analysis is based on modelling the airfoil surface with source and vortex sheet and this sheet is approximated by a series of straight panels. The concentration of panels on this sheet is more near the leading and trailing edges. The midpoint of each panel is called a control point $\left(\bar{x}_i\ ,\bar{y}_i\right)$ at which the boundary conditions [see Appendix for details] are applied. At each control point, the normal component of velocity V_{ni} is zero and the tangential component of the velocity V_{ti} is calculated. Then the coefficient of pressure (C_p) at the control point of each panel is calculated as:

$$C_p\left(\bar{x}_i\ ,\bar{y}_i\right) = 1 - \frac{{V_{\mathrm{ti}}}^2}{{\mathrm{V}_\infty}^2} \tag{3.18}$$

For an inviscid, incompressible flow the aerodynamic force coefficients on an airfoil are computed as integrals of the pressure distribution over the body [see Appendix for details].

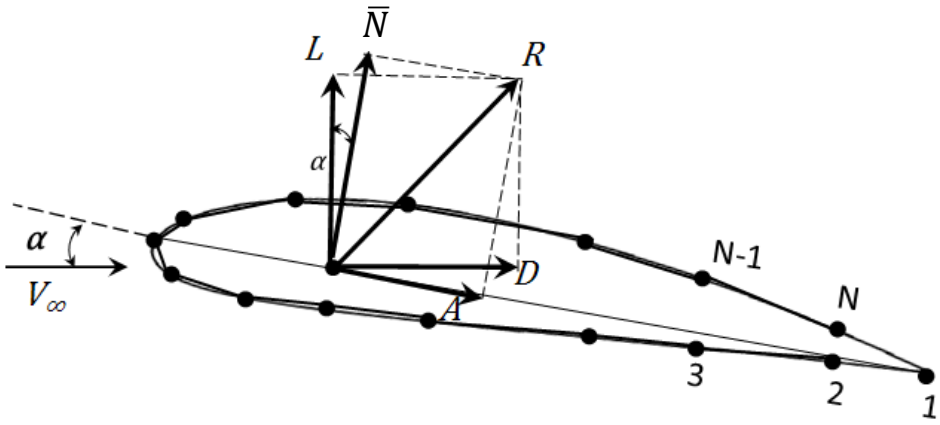

Figure 4. Resultant aerodynamic force and the components into which it splits

From Figure 4, it can be observed that the *net steady* force acting on the airfoil from integrated pressure distributions is denoted by *R,* the orthogonal components of which are $\bar{N}$ and *A,* normal to and along the chord line respectively. The orthogonal components of this force *R* are also given by the lift *L* and drag *D*, that are respectively normal to and along the free stream flow direction (*i.e.* V_∞). These sets of the components are related by the following expression:

$$\begin{Bmatrix} L \\ D \end{Bmatrix} = \begin{bmatrix} cos\alpha & -sin\alpha \\ sin\alpha & cos\alpha \end{bmatrix} \begin{Bmatrix} \bar{N} \\ A \end{Bmatrix} \tag{3.19}$$

The pitching moment on the airfoil about the support point O is given by

$$M = \bar{N}\,(X_o - X_{cp}) \tag{3.20}$$

Note that for very small angles of attack, $\sin\alpha \approx 0, \cos\alpha \approx 1$. Therefore, for small angles of attack, it is reasonable to assume that $\bar{N} \approx L$. Hence the pitching moment can be approximated as $M = L(X_o - X_{cp})$.

We now try to model the unsteady aerodynamic loads for small dynamic perturbations from the mean or steady flow. We assume that for low subsonic flows, and for very small angles of attack, (both mean and steady), the unsteady aerodynamic forces are governed solely by the unsteady perturbations about the mean steady configuration through simple linear relationships, and the effects of steady configurations upon unsteady forces are negligibly small. With this assumption, and without loss of generality, we now assume for convenience that the unsteady aerodynamic loads are produced solely through small unsteady perturbations about the mean position. Thus in Figure 4, we interpret α as the small unsteady (oscillatory) angle of attack as perturbation about the steady configuration that corresponds to a zero mean angle of attack (α_{mean} = 0). This implies that the unsteady α (of small value) is measured from the line of relative steady flow V_∞. Furthermore, for small values of unsteady angles of attack, $\bar{N} \approx L$. Hence the unsteady pitching moment can be approximated as $M = L(X_o - X_{cp})$, *i.e.* contribution to pitching moment is approximated to be from the unsteady lift alone, provided the unsteady angles of attack about the mean are very small. In low subsonic linear aerodynamic flow regime, this is a good approximation even for small non zero mean angles of attack. The unsteady aerodynamic forces and the structural response of the airfoil presented here are effectively dynamic perturbations about the mean values.

The incompressible aerodynamic forces are corrected by Prandtl-Glauert compressibility correction factor for subsonic compressible flow. The Prandtl-Glauert compressibility correction factor is $\sqrt{1 - M_\infty^2}$; where $M_\infty = \frac{V_\infty}{\sqrt{\gamma R T_\infty}}$ is the free stream Mach number. For calculating the aerodynamic forces using panel method a FORTRAN code is developed which requires total number of nodes, coordinates of each node, angle of attack (α), free stream velocity, density (ρ_∞) and temperature (T_∞) as inputs. The position of centre of pressure for different angle of attack is also obtained from this code and it is observed that these values lie near the quarter chord point for the given airfoil.

3.2.2 Assumed lift gradient and centre of pressure at quarter chord point (c/4)

In this method the aerodynamic forces (L and M) are calculated by taking $dC_L/d\alpha = \frac{2\pi}{\sqrt{1-M_\infty^2}}$, but no pressure distribution over the airfoil is actually computed. For the case where aerodynamic damping is ignored, equations (2.4) and (2.5) are used with ($\alpha_{eff} = \alpha$). Note that these forces are obtained by assuming that the position of centre of pressure lies at quarter chord point (*i.e.* $X_{cp} = c/4$).

3.2.3 Time integration algorithm

Having obtained aerodynamic forces, the above equation is solved numerically using Newmark's algorithm. Here, with discrete time steps, *i.e.* each of Δt, the displacement vector $\{u_{i+1}\}$ and the velocity vector $\{\dot{u}_{i+1}\}$ at time t_{i+1} are calculated from the expressions given below

$$\{u_{i+1}\} = \{u_i\} + \{\dot{u}_i\}\Delta t + \frac{\Delta t^2}{2}\{\ddot{u}_i\} \tag{3.21}$$

$$\{\dot{u}_{i+1}\} = \{\dot{u}_i\} + \frac{\Delta t}{2}[\{\ddot{u}_i\} + \{\ddot{u}_{i+1}\}] \tag{3.22}$$

The expression for the equation of motion at time t_{i+1} can be written as:

$$[\mathcal{M}]\{\ddot{u}_{i+1}\} + [D]\{\dot{u}_{i+1}\} + [K]\{u_{i+1}\} = \{F_{i+1}\} \tag{3.23}$$

The above expression can be rearranged to get the acceleration at time t_{i+1} as:

$$\{\ddot{u}_{i+1}\} = \left[[\mathcal{M}] + \frac{\Delta t}{2}[D]\right]^{-1}\left[\{F_{i+1}\} - [K]\{u_{i+1}\} - [D]\left[\{\dot{u}_i\} + \frac{\Delta t}{2}\{\ddot{u}_i\}\right]\right] \tag{3.24}$$

The force vector $\{F_{i+1}\}$ at time $\{t_{i+1}\}$ is now obtained by either running panel code that stimulates the unsteady aerodynamics for the given condition or using constant $dC_L/d\alpha$. A flow chart to calculate the dynamics of the airfoil using Newmark's algorithm has been explained in Figure 5.

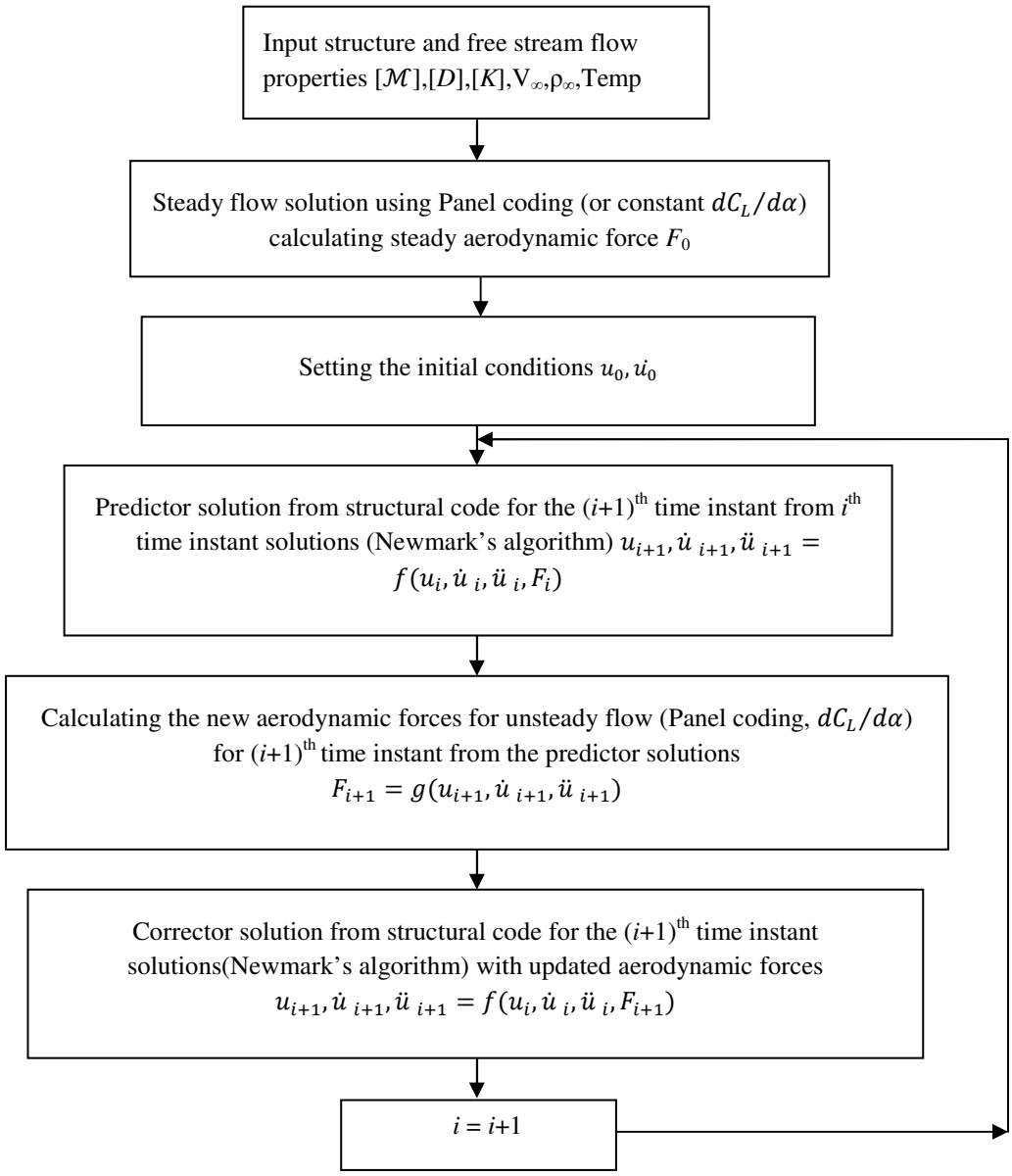

Figure 5. A flow chart to calculate the dynamics of the airfoil using Newmark's algorithm

Explanation of the algorithm

C The initial displacement and velocities are fed into the panel code from where the forces are calculated which are fed into the structural Subroutine

IF(IT.EQ.1) THEN	IT is the time step
F(1)=SLIFT	Lift
F(2)=SMOM	Moment

```
      D(1)=HI                                  Heave displacement
      D(2)=AI*PI/180                           Pitch displacement
      V(1)=HVI                                 Heave velocity
      V(2)=AVI                                 Pitch velocity
C
C     **** EVALUATION OF INITIAL ACCELERATION******
C
      DO 88 I=1,2
      ACC(I)=0.0
      DO 89 J=1,2
      ACC(I)=ACC(I)+SMI(I,J)*FACT(J)           Initial acceleration
89    CONTINUE
88    CONTINUE
C
      DO I=1,2
      ACCU(I)=0.0
      ACCU(I)=ACC(I)
      ENDDO
C
      ENDIF
C     ----------First loop ends here for IT=1-------------------------------
      DO I=1,2
      ACC(I)=ACCU(I)
      ENDDO
C
      DO 44 I=1,2
       D(I)=D(I)+V(I)*DELT+(DELT*DELT)*ACC(I)/2          Calculating updated
                                                        displacements for next time step
44    CONTINUE
C
      ALPHA=D(2)
C
      CALL PANEL(ALPHA,IT)                     Subroutine panel called to update the
                                               forces for the given time step


      F(1)=SLIFT
      F(2)=SMOM
C
C     UPDATED ACCELERATION USING RELATION:
C
```

$$\left\{\ddot{u}_{i+1}\right\} = \underbrace{\left[[M]+\frac{\Delta t}{2}[D]\right]^{-1}}_{\text{DMINV}} \underbrace{\left[\{F_{i+1}\}-[K]\{u_{i+1}\}-[D]\left(\left\{\dot{u}_i\right\}+\left\{\ddot{u}_i\right\}\frac{\Delta t}{2}\right)\right]}_{\text{FACT1(I)}}$$

```
C
C
```

```
C
      DMSUM(1,1)=SM(1,1)+.5*DELT*DC(1,1)
      DMSUM(1,2)=SM(1,2)
      DMSUM(2,1)=SM(2,1)
      DMSUM(2,2)=SM(2,2)+.5*DELT*DC(2,2)
C
C
      DETMD=DMSUM(1,1)*DMSUM(2,2)-DMSUM(1,2)*DMSUM(2,1)
C
      DMINV(1,1)=DMSUM(2,2)/DETMD
      DMINV(1,2)=-DMSUM(2,1)/DETMD
      DMINV(2,1)=-DMSUM(1,2)/DETMD
      DMINV(2,2)=DMSUM(1,1)/DETMD
C
      DO 77 I=1,2
      FACT1(I)=F(I)-ST(I,I)*D(I)-DC(I,I)*(V(I)+(DELT*ACC(I)/2))
77    CONTINUE

      DO 66 I=1,2
      ACCU(I)=0.0
      DO 67 J=1,2
      ACCU(I)=ACCU(I)+DMINV(I,J)*FACT1(J)          Updated acceleration
67    CONTINUE
66    CONTINUE

C   UPDATED VELOCITY CALCULATION
C
      DO 55 I=1,2
      V(I)=V(I)+0.5*DELT*(ACC(I)+ACCU(I))          Updated velocity
55    CONTINUE
C
      RETURN
      END
```

$$\underbrace{\left[[M]+\frac{\Delta t}{2}[D]\right]}_{\text{DMSUM}}$$

4. ANALYSIS OF A TYPICAL AIRFOIL

In this section the dynamic analysis is performed for a typical airfoil section (Figure 2) with the properties given in Table 1, using the methods outlined in the last section.

Table 1. *Properties of the airfoil*

Geometry	Chord, c = 1m, Position of support X_O =0.4 m, Profile: NACA 0012 airfoil (*symmetric*).
Inertia	Mass m=51.5 Kg, Moment of inertia about support O , I_α = 2.275 Kg m^2 Position of Center of Mass, X_{cm} =0.4429 m Distance of center of mass from support, X_A =0.0429 m X_A/c=0.0429 , $\sqrt{\frac{I_\alpha}{mc^2}} = 0.2102$ Moment of inertia of airfoil about the centre of mass $I_{cm} = I_\alpha - mX_A^2 = 2.1802 \text{ kg } m^2$ Moment of inertia about the centre of mass of a uniform section of unit length and chord c, and of mass m distributed *uniformly* is $\frac{mc^2}{12} = 4.2917\ kgm^2$. Since $I_{cm} < \frac{mc^2}{12}$, we conclude that most of the mass of the airfoil section is concentrated towards the central part of the airfoil.
Stiffness	Heave stiffness K_h =50828.463 N/m, Pitch stiffness K_α =35923.241 Nm/rad
Damping	Heave damping ratio, $\zeta_h = \frac{C_h}{2\sqrt{K_h m}} = 0.01$, Heave damping coefficient C_h =32.358 Ns/m Pitch damping ratio, $\zeta_\alpha = \frac{C_\alpha}{2\sqrt{K_\alpha I_\alpha}} = 0.01$ Pitch damping coefficient C_α =5.718Nms/rad

The values of above properties of the airfoil are just representative and do not conform to the actual values of the NACA 0012 airfoil but they are chosen such that it has a subsonic flutter boundary. The natural frequencies of the airfoil (un-damped) with the given support conditions are 4.9 Hz (30.79 radians/sec) and 20.45 Hz (128.49 radians/sec) for the primarily heaving mode and primarily pitching mode respectively.

4.1 Numerical results on flutter of an airfoil using classical method

4.1.1 Direct eigenvalue method for the undamped case

The results obtained by solving the eigenvalue problem defined by equation (3.3) and presented graphically in Figure 6. Flutter occurs when the two frequencies *coalesce,* at which point the eigenvalues become a complex conjugate pair. The stability conditions for this case are already presented in section 3.1.1.1. It is observed that the flutter frequency of the airfoil is 7.16 *Hz* and the corresponding flutter velocity is 175 m/sec.

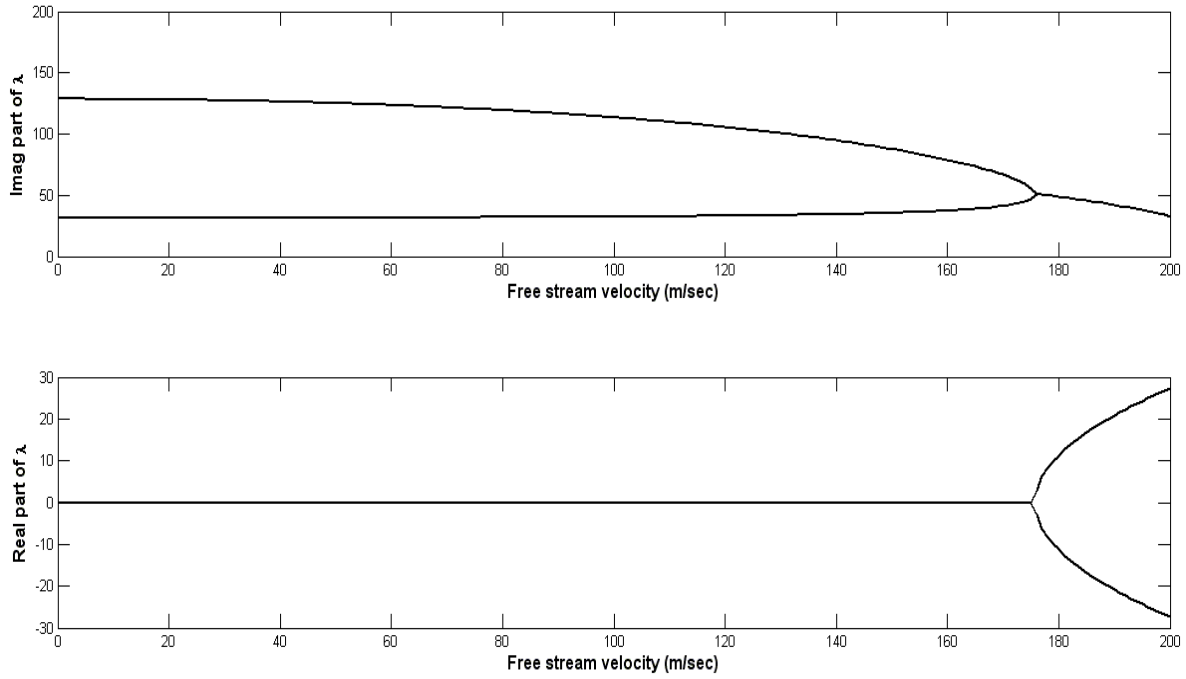

Figure 6. Real and Imaginary part of λ vs. free stream flow velocity V_∞ without any damping. The imaginary part λ_i denotes the circular frequency ω (in radians/sec) and the real part λ_r is related to stability. Beyond the critical velocity (175 m/sec), the real part of one root is positive, λ_r>0, indicating unstable oscillation.

4.1.2 State space method for the damped case

In the presence of damping, the flutter frequency and the corresponding velocity of the airfoil have been obtained by solving equation (3.13) using state space method. Figure 7 shows the imaginary and real parts of λ versus free stream flow velocity. The stability conditions for the damped case are already presented in section 3.1.1.2. The imaginary parts of the roots yield the circular frequencies (radians/sec) of the modal branches, while the real parts indicate decay/increase of amplitudes with time. It is observed that the critical (flutter) flow velocity is 189.7 m/sec. For flow regimes below this critical velocity, both the modal branches are damped, while for those beyond this velocity, one of the modal branches (of the higher frequency that displays softening tendencies with increase in flow velocity) shows unstable diverging oscillations with time.

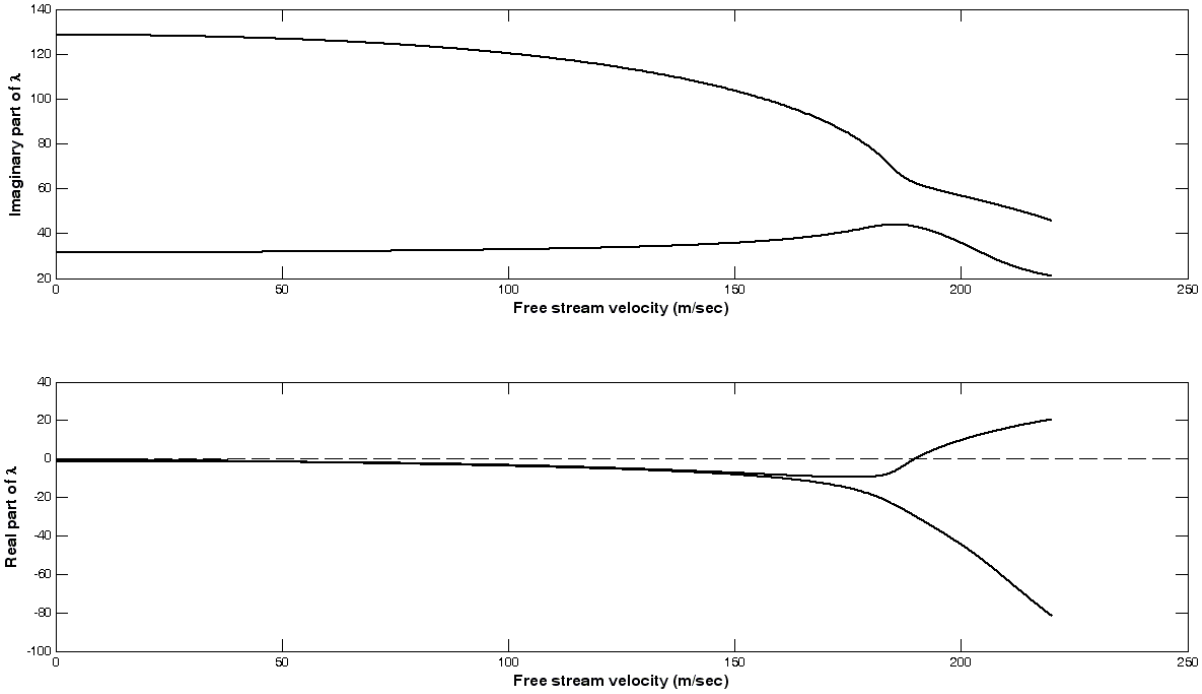

Figure 7. Real and Imaginary part of λ vs. free stream flow velocity V_∞ with both aerodynamic and structural damping, and incorporation of Theodorsen's function *C(k)*. The imaginary part λ_i denotes the circular frequency ω (in radians/sec) and the real part λ_r is related to the *net* damping in the form $\lambda_r = -\zeta\omega$. Beyond the critical velocity (189.7 m/sec), the real part of one root is positive, $\lambda_r > 0$, indicating unstable oscillation.

4.2 Steady results from in-house developed panel code for NACA 0012 Airfoil

In this section, steady results for *NACA 0012* airfoil are presented using panel method. These steady results are obtained to validate the present panel code with the available analytical solutions for subsonic incompressible and non-viscous flows.

The pressure distributions (C_p) along the chord length of the airfoil with different angles of attack are presented in Figure 8. From the figures it is observed that at $\alpha = -2^0$ the stagnation point* is on the upper surface of the airfoil and hence the lift is negative. At $\alpha = 0^0$ the net area enclosed by the curve of C_p against X/c is found to be zero. However at $\alpha = 2^0$ the stagnation point is now on the lower surface of the airfoil and hence the lift is positive. On further increase in the angle of attack ($\alpha = 6^0$), the pressure peak on the upper surface increases and moves towards the leading edge of the airfoil. However there is not much change in the shape (or profile) of the pressure distribution on the lower surface of the airfoil, though this profile gets somewhat shifted along the C_p axis.

The variation of lift and moment coefficients about the leading and trailing edges with different angle of attack are shown in Figures 9 and 10 respectively. It can be observed that both the lift and moment coefficients vary linearly with the angle of attack.

*It is a point at which the value of C_p is unity.

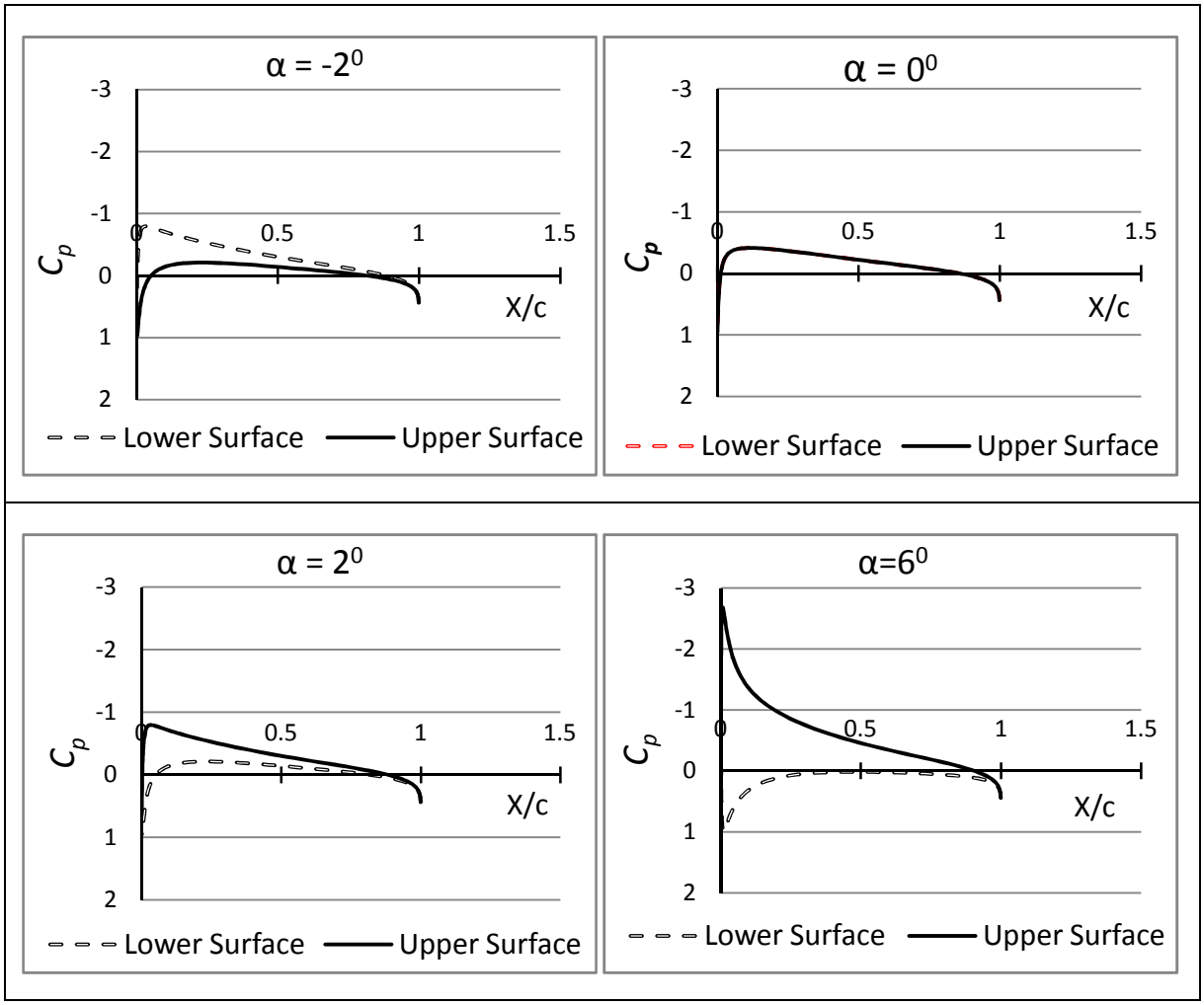

Figure 8. Pressure distributions on airfoil

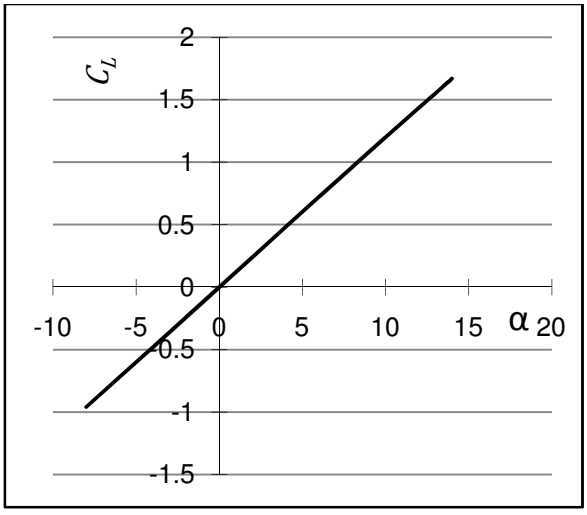

Figure 9. C_L vs. α curve

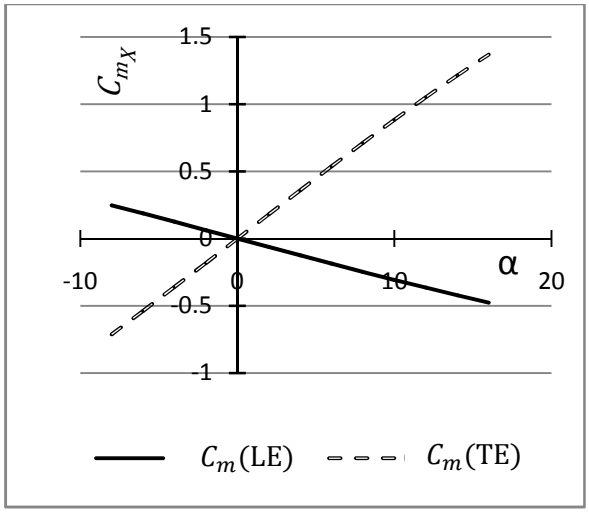

Figure 10. C_m vs. α curve

4.3 Dynamic response of the NACA 0012 airfoil to aerodynamic forces generated through the steady panel code, (and also with an assumed lift gradient)

In this section the dynamics of *NACA 0012* airfoil, with only structural/viscous damping is studied under different air flow conditions. The results are obained by coupling the in-house developed panel code with the structural code using the Newmark's algorithm. For any transient angle of attack of the airfoil, the panel code simulates the pressure distribution on the airfoil which is later used to calculate the airodynamic lift and moment in time at the flexural point of the airfoil. These lift and moment are then passed to the structure code to estiamte the response of the airfoil. The structural data taken in this study are same as defined in section 4.1. Here, the structural damping ratios ($\zeta_h = \frac{C_h}{2\sqrt{K_h m}}$ =0.01and $\zeta_\alpha = \frac{C_\alpha}{2\sqrt{K_\alpha I_\alpha}}$ =0.01) are also taken into account. No unsteady effects in the aerodynamics are incorporated here. These unsteady effects can be incorporated by a suitable unsteady aerodynamic code that may be coupled to the airfoil structureal code in future.

The variation of the time history of the dynamic response (heave and pitch) of the airfoil at the point of support and the corresponding aerodynamic lift and moment coefficients are obtained through the code with panel code generating the aerodynamic forces on the NACA 0012 airfoil. The results for various free stream air flow velocities are presented in Figures 11 to 14.

From Figures 11 and 12, it is observed that the displacements and aerodynamic forces oscillate and converge to zero mean position of the airfoil with time for flow velocities below the flutter boundary (viz. 140 m/sec and 160 m/sec). From Figure 13, it is evident that at the critical flow velocity of 161.3 m/sec, the amplitudes neither decay nor increase with time. Figure 14 shows that at a flow velocity of 163 m/sec (beyond the critical velocity), the amplitudes of the diplacements and aerodynamic forces increase with time. The results thus indicate that the oscillations of the airfoil under flow velocities below 161.3 m/sec is stable, and those beyond this critical velocity are unstable.

Similar results are also obtained for the identical airfoil with aerodynamic forces generated through a code with an assumed lift gradient ($dC_L/d\alpha$) and center of pressure at quartre chord point. For this case, the response at the critical flow velocity (174.2 m/sec) only is presented in Figure 14.

The results obtained for the typical airfoil using the classical methods have been compared with those obtained by time simulation based direct integration approach, with the generation of the aerodynamic forces, using two menthods; the panel method based on integrated pressure distribution, and the one with assumptions of constant lift gradient ($dC_L/d\alpha$) and centre of pressure at quarter chord point. Table 2 shows the flutter velocities obtained by various methods.

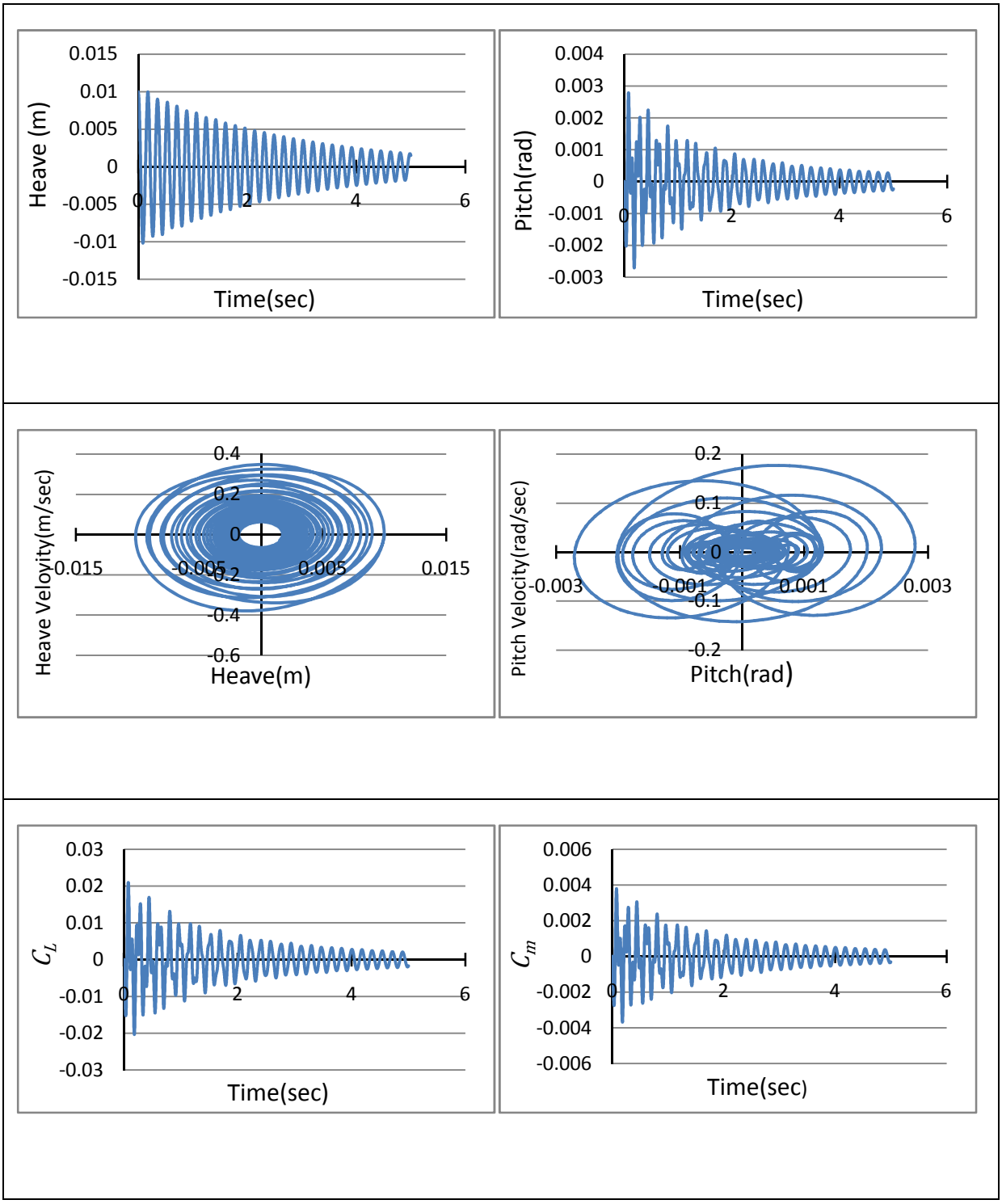

Figure 11. Time history and phase portrait of displacement and aerodynamic forces at the support point of the airfoil with free stream flow velocity 140 m/sec (M_∞ = 0.411, ρ_∞ = 1.2256 kg/m^3) using *panel code*. Initial conditions (at t=0): h = 0.01 m, dh/dt = 0.001 m/sec, α =0 rad, and $d\alpha/dt$ = 0.01 rad/sec.

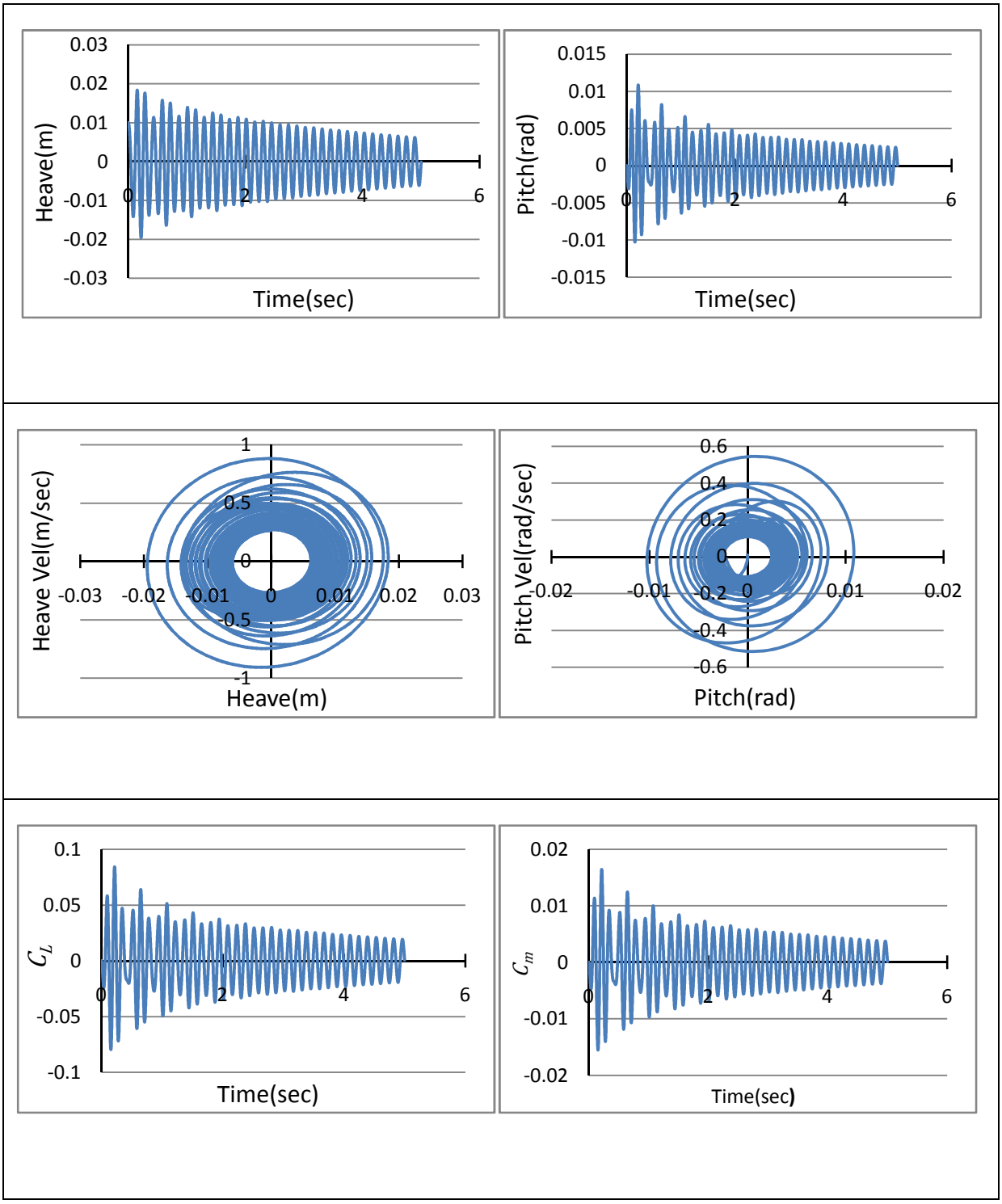

Figure 12. Time history and phase portrait of displacement and aerodynamic forces at the support point of the airfoil with free stream flow velocity 160 m/sec (M_∞ = 0.470, ρ_∞ = 1.2256 kg/m^3) using *panel code*. Initial conditions (at t=0): h = 0.01 m, dh/dt = 0.001 m/sec, α =0 rad, and $d\alpha/dt$ = 0.01 rad/sec.

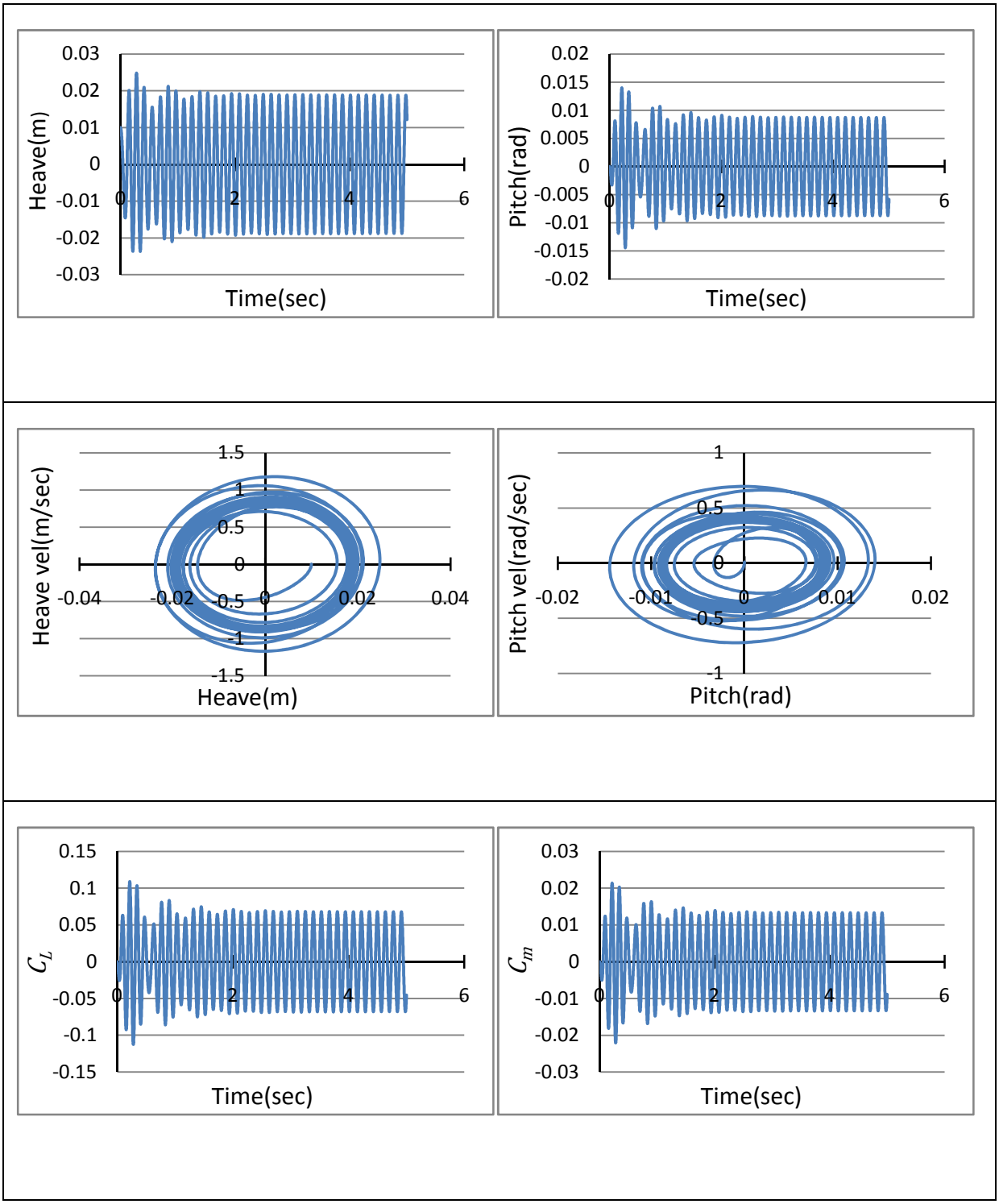

Figure 13. Time history and phase portrait of displacement and aerodynamic forces at the support point of the airfoil with free stream flow velocity 161.3m/sec (M_∞ = 0.474, ρ_∞ = 1.2256 kg/m^3) using *panel code*. Initial conditions (at t=0): h = 0.01 m, dh/dt = 0.001 m/sec, α = 0 rad, and $d\alpha/dt$ = 0.01 rad/sec.

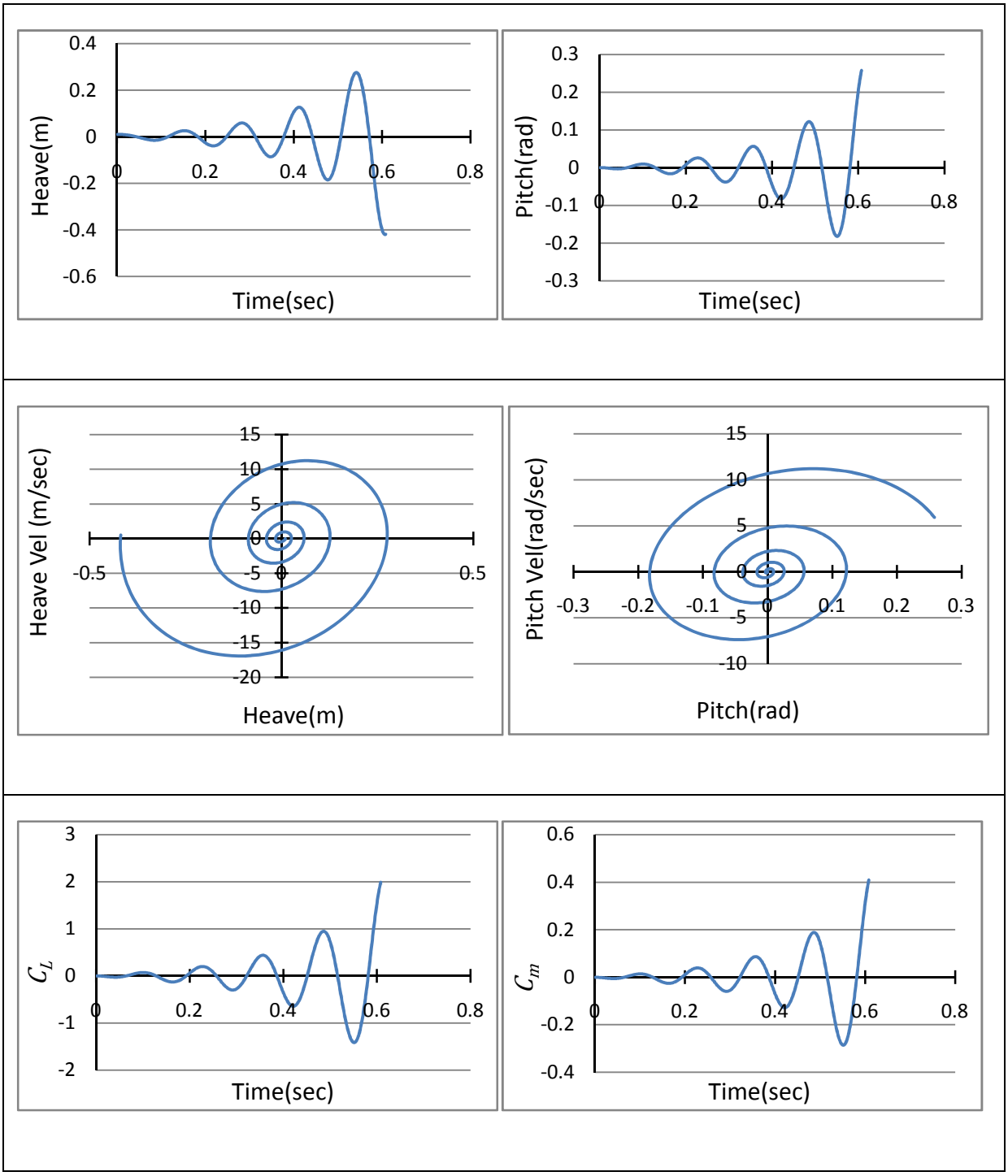

Figure 14. Time history and phase portrait of displacement and aerodynamic forces at the support point of the airfoil with free stream flow velocity 163 m/sec (M_∞ = 0.479, ρ_∞ = 1.2256 kg/m^3) using *panel code.* Initial conditions (at t=0): h = 0.01 m, dh/dt = 0.001 m/sec, α = 0 rad, and $d\alpha/dt$ = 0.01 rad/sec.

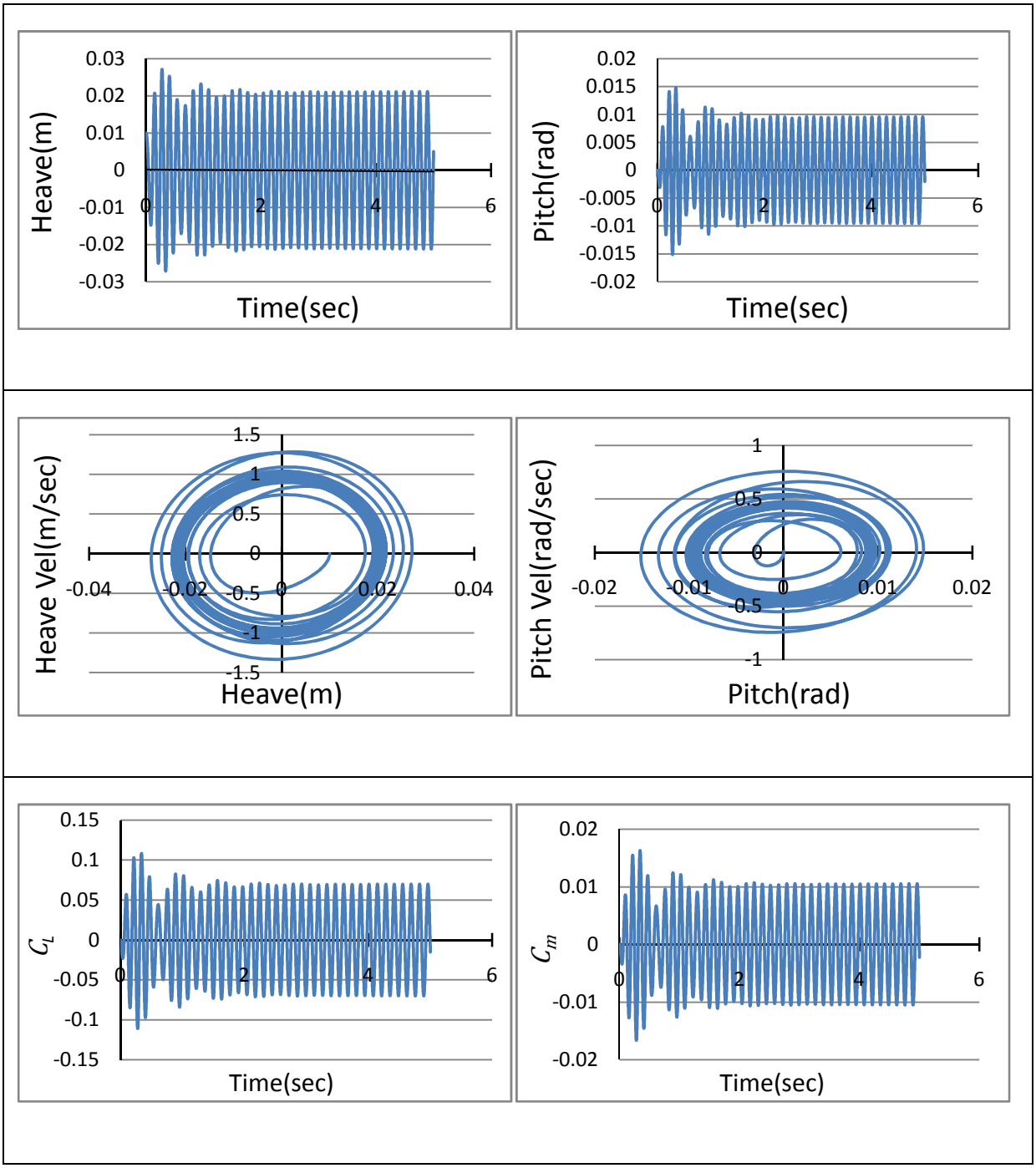

Figure 15. Time history and phase portrait of displacement and aerodynamic forces at the support point of the airfoil with free stream flow velocity 174.2 m/sec (M_∞ = 0.512, ρ_∞ = 1.2256 kg/m^3) using assumed lift gradient $\frac{dC_L}{d\alpha} = \frac{2\pi}{\sqrt{1-M_\infty^2}}$ and assumed center of pressure at quarter chord point (c/4). Initial conditions (at t=0): h = 0.01 m, dh/dt = 0.001 m/sec, α = 0 rad, and $d\alpha/dt$ = 0.01 rad/sec.

Table 2*: Flutter velocity of the airfoil using different methods*

METHOD	FLUTTER VELOCITY
Classical direct eigenvalue approach, without any damping	175 m/sec (Figure 6)
Classical method (State Space approach) with aerodynamic and structural damping and Theodorsen's function *C(k)*	189.7m/s (Figure 7)
Time domain, with only structural damping, using Panel code for generation of aerodynamic forces from integrated C_p distribution on NACA 0012 airfoil	161.3m/s (Figure 13)
Time domain, with only structural damping, with a code to generate aerodynamic forces with assumed lift gradient $\left(\frac{dC_L}{d\alpha} = \frac{2\pi}{\sqrt{1-M_\infty^2}}\right)$ and assumed center of pressure at c/4	174.2m/s (Figure 15)

5. OBSERVATIONS

5.1 Discussion of results

In the previous sections, the dynamic response of a typical NACA 0012 airfoil was studied using both the direct integration and the eigen value approaches. The objective of this whole study was to simulate the dynamic behaviour of a given airfoil at different airflow velocity. First the direct eigen value based analytical approach has been used to predict flutter of a typical undamped airfoil. An analytical approach based on state space method has also been introduced to study the flutter of a damped airfoil including both structural and aerodynamic damping. Here, the phase difference between the aerodynamic forces and the airfoil response are simulated using a frequency dependent Theodorsen's complex function $C(k)$ and the *p-k* method is adopted for solution. The flutter velocity obtained using the classical approaches for the damped airfoil is found to be *higher* than that for the undamped airfoil system (see Table 2). The analytical approach uses the assumed lift gradient assumption for generating aerodynamic forces.

In real time simulation, a CFD method based aeroelastic analysis has been done to simulate the dynamic response of a given airfoil. Here two different methods (panel method for generating the C_p distribution and load, and a second method based on assumed lift gradient assumption $dC_L/d\alpha$ with center of pressure at quarter point chord) are used for caluclating the aerodyamic forces acting on the airfoil. Here, only the structural damping is taken into account. It has been observed that

(i) The airfoil oscillates (both heave and pitch motions) and converge to zero mean position of the system with time at air flow velocity of 140 m/sec. At flow velocity of 161.3 m/sec, both the heave and pitch motions of the airfoil are simple harmonic in nature and their amplitudes remain constant with time. This also shows that the airfoil has just reached the neutrally stable condition (flutter). However, at flow velocity of 163 m/sec, the airfoil oscillates unboundedly whose amplitudes increase exponentially with time. This shows that the motion of the airfoil at this flow velocity is unstable.

(ii) The flutter velocity obtained by time domain approach using the panel method is slightly lower (161.3 m/sec) compared to the value (174.2 m/sec) obtained by the second method based on an assumed lift gradient value ($dC_L/d\alpha$) with center of pressure at quarter point chord. This happens because of the higher lift gradient with respect to the pitch angle obtained through the panel code over the NACA 0012 airfoil.

(iii) The present work is based on a panel code meant for generating only steady flows around any chosen airfoil profile. This steady code has been used in a real time loop to simulate aerodynamic loads the dynamic nature of which is dictated by the dynamic variation of the pitch angle only. This panel code cannot generate actual unsteady flow effects, and hence the results are only approximate. However, efforts are being made to develop a code for generating the unsteady aerodynamic loads for simulating the airfoil dynamics in a truly unsteady aerodynamic flow. Further it is possible to simulate flutter even in the transonic and supersonic regimes, using more sophisticated aerodynamic codes (solving Navier Stokes equations).

5.2 Variation of flutter boundary with Mach number

For low subsonic flow, the variation of the critical dynamic pressure ($q_{\infty,cr}$) with change in free stream Mach number is obtained by the given relation

$$q_{\infty,cr} = Q\sqrt{1 - M_{\infty}^2} \tag{5.1}$$

where Q is the constant parameter that determines the flutter boundary for the airfoil. For the present simulation, the value of Q is 18107.39 as obtained from the flutter boundary using the panel code.

In Figure 16, the variation of critical dynamic pressure at different Mach number of NACA 0012 airfoil with the properties given in this report is presented. From the figure it is observed that as the Mach number of the airflow increases the critical dynamic pressure decreases and the curve exactly follows an elliptical path

$$\frac{q_{\infty,cr}^2}{Q^2} + M_{\infty}^2 = 1 \tag{5.2}$$

Here, the maximum Mach number upto which the above expression is approximately applicable is nearly equal to 0.7. Beyond this limit, the flow enters the transonic regime, in which it becomes very complex and non-linear. In the transonic regime, viscous effects become important. Because of the limitations of the panel code, we need more sophisticated CFD code to analyse the dynamic behaviour of the airfoil in the transonic and supersonic regimes.

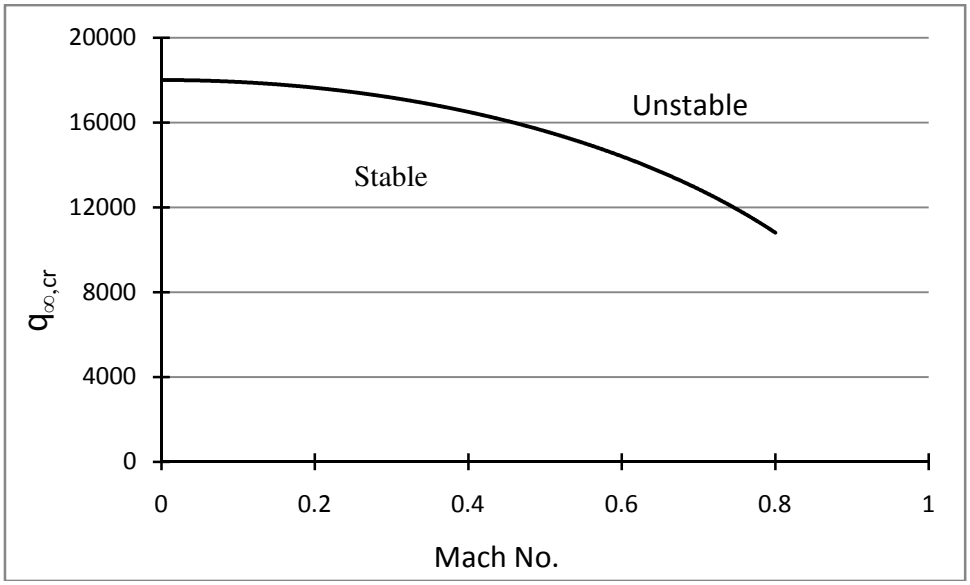

Figure 16. Variation of critical dynamic pressure with different free stream Mach number for a typical airfoil

6. CONCLUSIONS

In the present work, aeroelastic analysis of a typical airfoil has been done using three different methods. Classical eigenvalue approaches and direct integration methods have been employed to study the dynamic response and prediction of flutter boundaries of the airfoil. Good agreement has been observed between the values of the flutter velocity obtained by the various methods. The unsteady airfoil displacements (dynamic) are generated with reference to the corresponding mean/steady values as the datum. This was done with the assumption that the mean values do not affect the unsteady behavior of the system, and the aerodynamic forces are linear in the displacements. This is a reasonable assumption in the low subsonic flow. The present analysis with a simple airfoil coupled to a 2D subsonic flow (simulated by the panel method) also indicates that it is possible to simulate flutter even in the transonic and supersonic regimes, using more sophisticated aerodynamic codes (solving Navier Stokes equations).

REFERENCES

1. **Fung Y.C.** *An Introduction to the Theory of Aeroelasticity,* John Wiley and Sons Inc, 1955.

2. **Bisplinghoff R.L., Ashley H.** and **Halfman R.L.** *Aeroelasticity*, Addison-Wesley Publication, 1957.

3. **Anderson, John D. Jr.** *Fundamentals of Aerodynamics,* McGraw-Hill Book Company, First edition, 1988.

4. **Maron J.** *Introduction to Theoretical Computational Aerodynamics*, John Wiley, New York, 1984.

5. **Mukherjee S.** *An investigation of Transonic Limit Cycle Oscillations of Airfoils*, DLR Project Report No: IB 232-2006 J 01. Institute for Aeroelasticity, German Aerospace Centre (*Deutsche Zentrum für Luft und Raumfahrt*, DLR), *Bunsenstrasse* 10, 37073 *Göttingen*, Germany, 2006. Research supported by CSIR *Raman Research Fellowship*, June 1st 2005- February 28th 2006.

6. **Nitzsch J.** *Simulation des transsonischen Flatterns eines Tragflügelmodells im Zeitbereich* (Time domain simulation of transonic flutter of a wing model), Master's Thesis, *Technische Fachhochschule, Berlin*, Germany, 2005.

7. **Manjuprasad M., Sathish B. S., Viswanath S.** *Dynamic Aeroelastic Subsonic Discrete Gust Response Analysis of Lifting Surfaces in Time Domain using Newmark's Method*, NAL Project Report No: ST 0707, NAL, Bangalore, 2007.

8. **Burgal Padmakar A.** *Study of flutter Analysis of Airfoils and Wings*, Master's Thesis, NAL, Bangalore, 2007.

APPENDIX

Panel method for generation of aerodynamic forces on an airfoil subjected to non-viscous incompressible flow [3, 4]

It is a direct method for the numerical solution of nonlifting or lifting flows over arbitrary bodies or airfoils. It takes into account the following singularities (or boundary conditions) :

1. Flow tangency condition
2. Kutta condition

According to flow tangency condition the total velocity field should be tangent to the body surface and the normal component of velocity field must be zero. According to Kutta condition the flow leaves the trailing edge of a sharp tailed airfoil smoothly; that is, the velocity is finite there. In this technique potential function is taken as:

$$\emptyset = \emptyset_\infty + \emptyset_s + \emptyset_v \tag{A.1}$$

$$\emptyset_\infty = V_\infty(x\ cos\alpha\ +\ y \sin\ \alpha) \tag{A.2}$$

$$\emptyset_s = \int \frac{q(s) ln\ r\ ds}{2\pi} \tag{A.3}$$

$$\emptyset_v = -\int \frac{\gamma(s)\theta\ ds}{2\pi} \tag{A.4}$$

where $\emptyset_\infty$ is the potential of the uniform free stream flow having velocity V_∞, $\emptyset_s$ is the potential of source distribution of strength $q(s)$ per unit length, $\emptyset_v$ is the potential of vortex distribution of strength $\gamma(s)$ per unit length and α (angle of attack) is the inclination of the free stream flow velocity vector to the x-axis or chord line. Due to the superposition principle, $\emptyset$ automatically satisfies the *Laplace* equation and the boundary conditions at infinity. The source strength is governed by flow tangency condition at every control points. To satisfy this condition, the source strength must vary over the surface. The vortex strength is governed by the *Kutta* condition which involves only the trailing edge, therefore the vortex strength can be represented by a single number.

The integrals of equations (A.3) and (A.4) are hard to evaluate even for simple forms of source and vortex strengths, unless the surface on which the sources and vortices are distributed is a straight line. Thus we select a certain number '*N*' of points on the body contour, called nodes, and connect the nodes with straight lines, which represent the *panels* for the method as shown in the Figure (A.1).

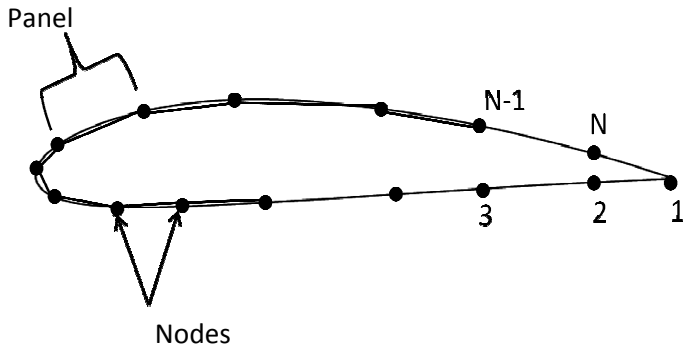

Figure A.1 Definition of Nodes and Panels

We then distribute the sources and vortices on the straight line panels, so that the potential given by equation. (A.1) may be written:

$$\emptyset = V_\infty(x\cos\alpha + y\sin\alpha) + \sum_{j=1}^{N} \int_{\text{Panel j}} [\frac{q(s)}{2\pi} \ln r - \frac{\gamma}{2\pi}\theta]\, ds \qquad (A.5)$$

In most cases, equation (A.5) still allows an exact solution of the flow problem. The exceptional cases are those in which the sources and vortices must be distributed exactly on the body surfaces. Even those cases can be well approximated by equation (A.5) simply by increasing the panel density so that the polygon formed by the panels better approximates the body shape. We must now assume some parameterized form for the variation of the *source* strength over the panels so as to be able to evaluate the integrals of equation (A.5) in terms of the parameters. This is the only major approximation of the Panel Method, one that becomes more accurate as the number of panels increases. We take the source strength to be constant on each panel, but variable from one panel to the next:

$$q(s) = q_i \text{ on panel } i, \qquad i=1.....N \qquad (A.6)$$

The parameters to be determined are then the N source strengths q_i and the vortex strength γ. For constant source and vortex strengths, the velocity is infinite at the end of each panel. This excludes the nodes from consideration as control points. The next most reasonable choice would be the points on the body midway between each adjacent pair of nodes. However, for constant strength source and vortex panels, it is just as accurate, and more convenient, to set the velocity component (V_{ni}) normal to each panel equal to zero at its midpoint. Similarly, for the Kutta condition, we equate the velocity components (V_{ti}) tangential to the panels adjacent to the trailing edge, again evaluating the components at the midpoint of the panels. If the lengths of the two trailing-edge panels are kept nearly equal as the number of panels is increased, this amounts to a requirement that the velocities at equal distances from the trailing edge approach one another as those distances are decreased (it is a corollary of the Kutta condition: near the trailing edge, the flow velocities on the upper and lower surfaces of the airfoil are equal at equal distances from the trailing edge).

To implement this method, we need some nomenclature. Let the i^{th} panel be defined as the one between the i^{th} and $(i+1)^{th}$ nodes, and its inclination to the x axis be θ_i, as shown in Figure (A.2).

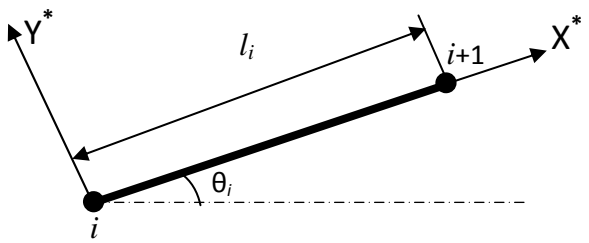

Figure A.2 Coordinate system fixed to the i^{th} panel

Here, $\hat{n}_i = -\sin\theta_i\,\hat{\imath} + \cos\theta_i\hat{\jmath}$ is the unit vector normal to the i^{th} panel (A.7)

and $\hat{t}_i = \cos\theta_i\,\hat{\imath} + \sin\theta_i\hat{\jmath}$ is the unit vector tangent to the i^{th} panel (A.8)

where $sin\theta_i = \frac{y_{i+1}-y_i}{l_i}$, $cos\theta_i = \frac{x_{i+1}-x_i}{l_i}$ and l_i is the length of i^{th} panel.

Now let the coordinates of midpoint of the i^{th} panel be:

$$\bar{x} = \frac{x_i+x_{i+1}}{2}\ ;\quad \bar{y} = \frac{y_i+y_{i+1}}{2} \tag{A.9}$$

The velocity components at these points are:

$$u_i = u(\bar{x}_i, \bar{y}_i)\ ; v_i = v(\bar{x}_i, \bar{y}_i)$$

$$\vec{V}_i = u_i\,\hat{\imath} + v_i\hat{\jmath}$$

The flow tangency condition can be written as:

$$V_{ni} = \vec{V}_i.\hat{n}_i = 0 \qquad \text{or}$$

$$0 = -u_i\sin\theta_i + v_i\cos\theta_i \qquad \text{for } i = 1 \ldots N \tag{A.10}$$

and the Kutta condition as

$$\vec{V}_1\hat{t}_1 = -\vec{V}_N.\hat{t}_N$$

$$u_1cos\theta_1 + v_1sin\theta_1 = -u_Ncos\theta_N - v_Nsin\theta_N \tag{A.11}$$

where suffix 1 refers to the trailing edge.

The minus sign in equation (A.11) are due to the definition of the tangential direction; $\hat{t}_1$ goes away from the trailing edge, and $\hat{t}_N$ toward it. The velocity component at the middle of the i^{th} panel, u_i and v_i are made up of contributions from the onset flow, the sources and the vortices on each panel. Because the velocities induced by the sources and vortices on a panel are u_s proportional to the source or vortex strength on that panel, we can write

$$u_i = V_\infty cos\alpha + \sum_{j=1}^{N}(q_j)\,u_{sij} + \gamma\sum_{j=1}^{N}u_{vij} \tag{A.12}$$

$$v_i = V_\infty sin\alpha + \sum_{j=1}^{N}(q_j)\,v_{sij} + \gamma\sum_{j=1}^{N}v_{vij} \tag{A.13}$$

where u_{sij} and v_{sij} are the x and y component of the velocity respectively, at the midpoint of the i^{th} panel due to a unit strength source distribution on the j^{th} panel. Similarly, u_{vij} and v_{vij} are the x and y components of the velocity respectively, at the midpoint of the i^{th} panel due to a constant strength vortex distribution.

To evaluate u_{sij}, v_{sij}, u_{vij} and v_{vij}, it is convenient to work in coordinates (x^*,y^*) oriented with the j^{th} panel (see Figure A.3). The global velocity components can be evaluated as

$$u = u^* \cos\theta_j - v^* \sin\theta_j \qquad v = u^* \sin\theta_j + v^* \cos\theta_j \tag{A.14}$$

once we find the "local" components (u^*, v^*). The velocity components at (x_i, y_i) due to unit strength source distribution on the j^{th} panel can then be written as

$$u^*_{sij} = \frac{1}{2\pi}\int_0^{l_j} \frac{x^*-t}{(x^*-t)^2+y^{*2}}\,dt \quad \text{and} \quad v^*_{sij} = \frac{1}{2\pi}\int_0^{l_j} \frac{y^*}{(x^*-t)^2+y^{*2}}\,dt \tag{A.15}$$

in which (x^*, y^*) are the local coordinates corresponding to (x_i, y_i).

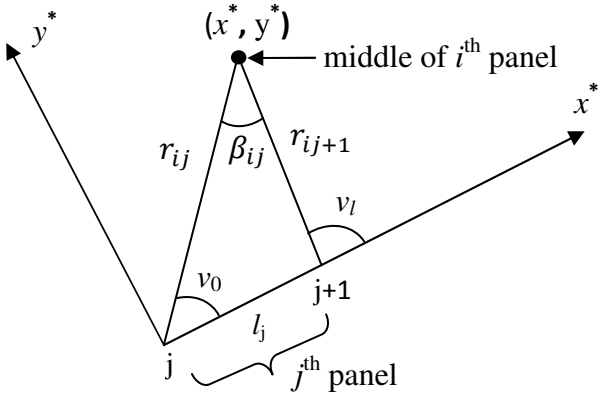

Figure A.3 Geometric interpretation of term β_{ij} for the velocity field of the constant strength source and vortex panels

Such results have a geometric interpretation, which obviates their translation back into the global coordinates. Referring to Figure A.3 for nomenclature, we write

$$u^*_{sij} = \frac{-1}{2\pi} ln \frac{r_{ij+1}}{r_{ij}} \tag{A.16}$$

$$v^*_{sij} = \frac{v_l - v_o}{2\pi}$$

$$= \frac{\beta_{ij}}{2\pi} \tag{A.17}$$

where r_{ij} is the distance from the j^{th} node to the middle of the i^{th} panel, whereas β_{ij} is the angle subtended at the middle of the i^{th} panel by the j^{th} panel. $u^*_{sii} = 0$, but the value of the y^* component of velocity induced by the source panel at its own midpoint is not so obvious. If the point (x^*, y^*) approaches the panel from outside the panels, $\beta_{ii} \to \pi$. However, if it approaches the panel from the other side, $\beta_{ii} \to -\pi$. Since the flow is outside the body, we are interested in working on the outside of the panels and set $\beta_{ii} = \pi$. A convenient expression for β_{ij} is then

$$\beta_{ij} = \pi \qquad \text{if} \quad i=j$$

$$\beta_{ij} = \tan^{-1} 2\left[\left(\bar{y}_i - y_{j+1}\right)\left(\bar{x}_i - x_j\right) - \left(\bar{y}_i - y_j\right)\left(\bar{x}_i - x_{j+1}\right) * \left(\bar{x}_i - x_{j+1}\right)\left(\bar{x}_i - x_j\right)\right.$$

$$\left. +\left(\bar{y}_i - y_j\right)\left(\bar{y}_i - y_{j+1}\right)\right] \quad \text{if} \quad i \neq j \tag{A.18}$$

The velocity induced at (x^*, y^*) by the *vortices* on the j^{th} panel is now easy to evaluate as:

$$u^*_{vij} = \frac{1}{2\pi}\int_0^{l_i} \frac{y^*}{(x^*-t)^2+y^{*2}}\,dt = \frac{\beta_{ij}}{2\pi} \tag{A.19}$$

$$v^*_{vij} = -\frac{1}{2\pi}\int_0^{l_i} \frac{x^*-t}{(x^*-t)^2+y^{*2}}\,dt = \frac{1}{2\pi} ln \frac{r_{ij+1}}{r_{ij}} \tag{A.20}$$

The flow tangency condition given by equation (A.10) may now be put into the form

$$\sum_{j=1}^{N} A_{ij} q_j + A_{i,N+1}\gamma = b_i \tag{A.21}$$

where, with the help of equations. (A.12) to (A.21)

$$A_{ij} = -u_{sij} sin\theta_i + v_{sij} cos\theta_i$$

$$= -u^*_{sij}\left(cos\theta_j sin\theta_i - sin\theta_j cos\theta_i\right) + v^*_{sij}\left(sin\theta_i sin\theta_j + cos\theta_i cos\theta_j\right)$$

So

$$2\pi A_{ij} = \sin\left(\theta_i - \theta_j\right) ln \frac{r_{ij+1}}{r_{ij}} + \cos\left(\theta_i - \theta_j\right)\beta_{ij} \tag{A.22}$$

and similarly,

$$2\pi A_{iN+1} = \sum_{j=1}^{N} \cos\left(\theta_i - \theta_j\right) ln \frac{r_{ij+1}}{r_{ij}} - \sin\left(\theta_i - \theta_j\right)\beta_{ij} \tag{A.23}$$

whereas $b_i = V_\infty \sin\left(\theta_i - \alpha\right)$ (A.24)

The Kutta condition (equation (A.11)) can be put in similar form:

$$\sum_{j=1}^{N} A_{N+1,j}\, q_j + A_{N+1,N+1}\gamma = b_{N+1} \tag{A.25}$$

and, after the same sort of manipulation, we find

$$2\pi A_{N+1,j} = \sum_{k=1,N} sin\left(\theta_k - \theta_j\right)\beta_{kj} - \cos\left(\theta_k - \theta_j\right) ln \frac{r_{kj+1}}{r_{kj}}$$

$$2\pi A_{N+1,N+1} = \sum_{k=1,N}\sum_{j=1}^{N} sin\left(\theta_k - \theta_j\right) ln \frac{r_{kj+1}}{r_{kj}} + cos\left(\theta_k - \theta_j\right)\beta_{kj}$$

$$b_{N+1} = -V_\infty \cos(\theta_1 - \alpha) - V_\infty \cos(\theta_N - \alpha) \tag{A.26}$$

Equations (A.21) and (A.25) comprise a set of N+1 equations in the unknowns q_i, i = 1 ..., N and γ. Once they are solved, we can compute the tangential velocity at the midpoint of each panel from

$$V_{\mathrm{ti}} = \mathrm{V}_\infty \cos(\theta_\mathrm{i} - \alpha) + \sum_{\mathrm{j}=1}^{\mathrm{N}} \frac{\mathrm{q_j}}{2\pi}\left[\sin(\theta_\mathrm{i} - \theta_\mathrm{j})\beta_{\mathrm{ij}} - \cos(\theta_\mathrm{i} - \theta_\mathrm{j})\ln\frac{\mathrm{r_{ij+1}}}{\mathrm{r_{ij}}}\right]$$

$$+\frac{\gamma}{2\pi}\sum_{j=1}^{N}\left[sin(\theta_i - \theta_j)ln\frac{r_{ij+1}}{r_{ij}} + cos(\theta_i - \theta_j)\beta_{ij}\right] \qquad \text{(A.27)}$$

Since normal component of velocity at the midpoint of each panel, $V_{ni} = 0$, the pressure coefficient at midpoint of each panel can then be calculated from the relation

$$C_p\left(\bar{x}_i\ ,\bar{y}_i\right) = \frac{p-p_\infty}{\frac{1}{2}\rho_\infty V_\infty^2} = 1 - \frac{{V_{\mathrm{ti}}}^2}{{\mathrm{V}_\infty}^2} \qquad \text{(A.28)}$$

where p_∞, ρ_∞ and V_∞ are the free stream pressure, density and velocity respectively and p is the local pressure at the control point.

The aerodynamic forces can be estimated by integrating the pressure distributions, obtained by assuming C_p constant over each panel.

$$C_n = \sum_{i=1}^{N} C_p\left(\bar{x}_i\ ,\bar{y}_i\right)dx \ \text{ and } \ C_a = \sum_{i=1}^{N} C_p\left(\bar{x}_i\ ,\bar{y}_i\right)dy \qquad \text{(A.29)}$$

where C_n and C_a are the components of pressure coefficient parallel to Y and X axis (along the chord line, Figure 4) respectively, then the final equations of the lift coefficient C_L and moment coefficient about the leading edge, $C_{M(LE)}$, are given below

$$C_L = C_n\, cos\alpha - C_a\, sin\alpha \qquad \text{(A.30)}$$

$$C_{M(LE)} = \sum_{i=1}^{N}\left[C_p\left(\bar{x}_i\ ,\bar{y}_i\right)dy\,\bar{y} + C_p\left(\bar{x}_i\ ,\bar{y}_i\right)dx\,\bar{x}\right] \qquad \text{(A.31)}$$

The obtained values are for subsonic incompressible inviscid flow and these values can be corrected by Prandtl-Glauert compressibility correction factor $\sqrt{1-M_\infty^2}$ for the subsonic compressible flow. Then the modified relations for compressible flow will be

$$C_p(\text{compressible}) = \frac{C_p(\text{incompressible})}{\sqrt{1-M_\infty^2}},$$

$$C_L(\text{compressible}) = \frac{C_L(\text{incompressible})}{\sqrt{1-M_\infty^2}}, \qquad \text{(A.32)}$$

and $C_m(\text{compressible}) = \frac{C_m(\text{incompressible})}{\sqrt{1-M_\infty^2}}$

SUMMARY

This method is based on modelling an airfoil surface with source and vortex sheet. This vortex sheet is approximated by *N* number of straight panels. The concentration of panels on this sheet is more near the leading and trailing edges than that at the middle region of the airfoil. The midpoint of each panel is called a control point at which the boundary conditions are applied. At each control point, the normal component of velocity V_{ni} is zero and the tangential component of the velocity V_{ti} is calculated. Here, the flow tangency conditions lead to a set of *N* linear simultaneous equations (each of unknown *source* strengths q_j, *j=1,2...N*, and a single unknown *vortex* strength γ), as given in equation (A.21):

$$\sum_{j=1}^{N} A_{ij} q_j + A_{i,N+1}\gamma = b_i \qquad (i=1,2...N) \qquad \text{(A.33)}$$

where $b_i = V_\infty \sin(\theta_i - \alpha)$ by equation (A.24), where θ_i is the inclination of the panel with respect to the chord line (Figure A2) and α is the angle of attack in radians. The expressions for the coefficients A_{ij} are given in equations (A.22) and (A.23). The above set of *N* linear equations has a total of *N* + 1 unknowns.

The Kutta condition (flow leaves the trailing edge smoothly) applied at the trailing edge provides the (*N*+1) th equation (A.25):

$$\sum_{j=1}^{N} A_{N+1,j}\, q_j + A_{N+1,N+1}\gamma = b_{N+1} \qquad \text{(A.34)}$$

Thus the above set of *N* +1 linear equations (A.33 and A.34) ultimately yields a matrix form from which the *N* +1 unknowns can be now determined.

$$\begin{bmatrix} A_{11} & A_{12} & \cdots & A_{1,N+1} \\ A_{21} & A_{21} & \cdots & A_{2,N+1} \\ \cdots & \cdots & \cdots & \cdots \\ A_{N,1} & A_{N,2} & \cdots & A_{N,N+1} \\ A_{N+1,1} & A_{N+1,2} & \cdots & A_{N+1,N+1} \end{bmatrix} \begin{Bmatrix} q_1 \\ q_2 \\ \vdots \\ q_N \\ \gamma \end{Bmatrix} = \begin{Bmatrix} b_1 \\ b_2 \\ \vdots \\ b_N \\ b_{N+1} \end{Bmatrix} \qquad \text{(A.35)}$$

Once these *N*+1 equations are solved, we can compute the tangential velocity V_{ti} at the midpoint of each panel from equation (A.27). Since the normal component of the velocity is zero at the midpoint of each panel, ($V_{\mathrm{ni}} = 0$), the pressure coefficient C_p at each control point is calculated using tangential velocity (V_{ti}) from equation (A.28). Finally, the various aerodynamic force components on the airfoil are estimated by assuming constant C_p over each panel, and then integrating the pressure distributions appropriately (using equations A.29-A.32).

DOCUMENTATION SHEET

	NATIONAL AEROSPACE LABORATORIES	**Class : Unrestricted** **No. of Copies : 20**

Title: Time domain simulation of airfoil flutter in the subsonic regime using fluid structure coupling through panel method.

Authors: Somenath Mukherjee, M Manjuprasad, Neeraj Kumar Sharma, Davinder Rana, Amit Kumar Onkar.

Coordinators: D V Venkatasubramanyam (HOD STTD), N G Vijaya Vittala

Advisor: Dr A. R. Upadhya (Director NAL).

Division : Structural Technologies Division | **NAL Project No. : S-8-523**

Document No. : SP-08 25 | **Date of Issue : December 2008**

Contents	39	**Pages**	20	**Figures**	2	**Tables**	8	**References**

External Participation : -

Sponsor : In-house project

Approval : Head, Structural Technologies Division

Remarks: The FORTRAN code related to this work is developed at the Structural Technologies Division (STTD) and handed over to the Computational and Theoretical Fluid Dynamics Division (CTFD) of NAL.

Keywords: Time domain airfoil response, aerodynamic forces, airfoil flutter boundary, Newmark's algorithm, fluid-structure coupling, panel method, classical state space method, strip theory and pk method, aerodynamic damping.

Abstract:

This report presents a brief theory of aeroelastic flutter of airfoils and the relevant algorithm for the development of a computer code in FORTRAN for dynamic *coupling* of the airfoil structure, in the time domain, to a two-dimensional *subsonic* aerodynamic flow, so that the aeroelastic motion can be simulated in the time domain and the flutter boundary be determined for a typical rigid airfoil (of heave and pitch degrees of freedom) in the subsonic flow. The relevant computer code with fluid structure coupling has been developed at the Structural Technologies Division (STTD) for the purpose.

The present work starts with a brief introduction to the fundamental concepts of airfoil flutter. The relevant equations of motion of the airfoil in subsonic airflow have been derived from the first principles. First, the classical method, based on the eigenvalue approach is used to solve the equations of motion and to determine the flutter boundary of the airfoil in the subsonic flow regime. A symmetric NACA 0012 airfoil profile of unit chord and width is chosen for analysis, with suitable spring stiffness and inertia values so that flutter instability can occur in the subsonic regime.

Results from the panel code for steady flow conditions over the NACA 0012 confirm the validity of the code. For the purpose of time domain flutter simulation the panel code with the Prandtl-Glauert compressibility correction factor is suitably coupled to the airfoil through a Newmark's implicit time integration scheme. Unsteady motion in the fluid-structure system is numerically simulated through the code with small initial conditions. Flutter boundary is indicated by the critical free stream flow speed (and dynamic pressure) beyond which oscillation amplitudes show divergence in time. Flutter frequencies and flutter velocities obtained by the various methods are then compared, and good agreement is observed. Present analysis with a simple airfoil coupled to a 2D subsonic flow (simulated by the panel method) indicate that it is possible, in principle, to simulate flutter even in the transonic and supersonic regimes, using more sophisticated aerodynamic codes (Navier Stokes).